universe

MDPI

Review

GRMHD Simulations and Modeling for Jet Formation and Acceleration Region in AGNs

Yosuke Mizuno [1,2,3]

[1] Tsung-Dao Lee Institute, Shanghai Jiao Tong University, Shanghai 201210, China; mizuno@sjtu.edu.cn
[2] School of Physics and Astronomy, Shanghai Jiao Tong University, Shanghai 200240, China
[3] Institut für Theoretische Physik, Goethe Universität, Max-von-Laue Str. 1, D-60438 Frankfurt am Main, Germany

Abstract: Relativistic jets are collimated plasma outflows with relativistic speeds. Astrophysical objects involving relativistic jets are a system comprising a compact object such as a black hole, surrounded by rotating accretion flows, with the relativistic jets produced near the central compact object. The most accepted models explaining the origin of relativistic jets involve magnetohydrodynamic (MHD) processes. Over the past few decades, many general relativistic MHD (GRMHD) codes have been developed and applied to model relativistic jet formation in various conditions. This short review provides an overview of the recent progress of GRMHD simulations in generating relativistic jets and their modeling for observations.

Keywords: accretion; accretion disk; black hole; relativistic jets; magnetohydrodynamics (MHD); radiative transfer; methods: numerical

Citation: Mizuno, Y. GRMHD Simulations and Modeling for Jet Formation and Acceleration Region in AGNs. *Universe* **2022**, *8*, 85. https://doi.org/10.3390/universe8020085

Academic Editors: Sergei B. Popov, Ziri Younsi and Zdeněk Stuchlík

Received: 27 November 2021
Accepted: 22 January 2022
Published: 28 January 2022

1. Introduction

Relativistic jets are amongst the most powerful astrophysical phenomena discovered to date. Their relativistic nature causes them to emit powerful and extremely time-variable radiation in all ranges of wavelength, from radio to gamma rays. This makes them detectable at cosmological distances. Relativistic jets are known to be launched as the result of accretion processes onto extremely compact objects such as black holes (BHs) in the presence of rotating accretion flows and magnetic fields. This makes relativistic jets a powerful tool to probe the environment of objects in extremely compact matter states, and the physics of high-energy plasmas and their magnetic fields on different scales.

In the accretion processes onto BHs, a substantial fraction of the gravitational binding energy of the accreting matter is released within tens of gravitational radii from the BH. This released energy supplies the powerful radiation. Since the radiated energy originates from the vicinity of the BH, a fully general relativistic treatment is essential for the modeling of these objects and the flows of plasma in their vicinity.

Several mechanisms of jet flow acceleration and collimation have been proposed. These includes gas-pressure acceleration, acceleration by radiation, and magnetohydrodynamic (MHD) processes (e.g., [1]). It is also possible that different mechanisms operate in different sources [2], or, otherwise, that different mechanisms are operating simultaneously [3]. Currently, the most promising mechanism is that the jets may arise from the combined effects of magnetic fields and rotation. The important mechanisms here are the Blandford–Znajek (BZ) [4] and the Blandford–Payne (BP) models [5,6]. In BP models, the jet is formed as a result of magnetocentrifugal acceleration of matter from the surface of an accretion disk. On the other hand, in the BZ model relativistic jets can be launched from the black hole magnetosphere by extracting rotational energy of BHs. From these two models, we believe the relativistic Poynting-flux-dominated (energy and angular momentum outflow carried predominantly by the electromagnetic field) jets are driven by rotational energy of the BHs as invoked in the BZ model, whereas the sub-relativistic matter-dominated jets/winds are

driven by rotational energy of accretion flow owing to a magnetocentrifugal mechanism as in the BP model. However, there can be other alternative mechanisms, such as the gradient of magnetic and gas pressure. If the jet has sufficiently large specific enthalpy and is overpressured, the relativistic jets can be powerfully boosted by the propagation of a rarefaction wave from the interface between jet and ambient medium (e.g., [7,8]).

The essential physics for AGN jets can now be captured in relativistic MHD (RMHD) simulations. In particular, in order to understand jet formation from the vicinity of BHs, general relativistic MHD (GRMHD) simulations are required. Over the past few decades, many GRMHD codes have been developed (e.g., [9–26]) employing the 3 + 1 decomposition of spacetime and conservative 'Godunov' schemes based on approximate Riemann solvers [27–29]. These codes are applied to study a variety of high-energy astrophysical phenomena. Some of these GRMHD codes incorporate radiation (e.g., [30–32]), and/or non-ideal MHD processes (e.g., [33–38]). In state-of-the-art GRMHD codes, full treatment of adaptive mesh refinement has been implemented (see [21,23–25]) which is useful for obtaining higher spatial resolution in particular interesting regions such as strong shocks, turbulence, and shear regions.

Depending on the mass accretion rate, a black hole accretion system can be found in various spectral states [39,40]. Some AGNs have radiative power L in excess of their corresponding Eddington luminosity ($L_{\rm Edd}$). At the Eddington luminosity, radiation forces balance the gravity of the central object. In accretion disk theory, one of the scale parameters is mass accretion rate, where the Eddington mass accretion rate is $\dot{M}_{\rm Edd} \equiv L_{\rm Edd}/\epsilon c^2$, where ϵ is radiative efficiency $\epsilon \equiv L/\dot{M}c^2$. In some supermassive BHs, including the primary targets of observations by the Event Horizon Telescope Collaboration (EHTC), i.e., Sgr A* and M87, their mass accretion rates are well below the Eddington accretion rate, $\dot{M} \ll 10^{-2}\dot{M}_{\rm Edd}$ [41,42]. In this regime, the accretion flow advects most of the viscously released energy into the BH rather than radiating it to infinity. Such optically thin, radiatively inefficient, and geometrically thick flows are so-called advection-dominated accretion flows (ADAFs, see [43–46]). Analytical and semi-analytical approaches are reasonably successful in reproducing the main features in the spectra of ADAFs (see, e.g., [47]). However, numerical GRMHD simulations are essential to gain an understanding of the detailed physical processes. The accreting gas in an ADAF is radiatively inefficient. Therefore, an ADAF is also referred to as a radiatively inefficient accretion flow (RIAF).

At higher mass accretion rates, $10^{-2} \leq \dot{M}/\dot{M}_{\rm Edd} \leq 1$, radiative cooling becomes effective and the inner accretion disk shrinks into an optically thick geometrically thin accretion disk (e.g., [44]). This state is the so-called standard thin accretion disk (e.g., [48,49]). In thin accretion disk theory, the disk angular momentum is transported by α viscosity and its spectrum is well described by thermal black-body radiation.

At super-Eddington accretion rates, $\dot{M}/\dot{M}_{\rm Edd} \geq 1$, accretion flows again become radiatively inefficient. As the optical depth is large, the photon diffusion timescale from the disk interior to the photo-sphere becomes longer than the accretion timescale. Thus, the photons are advected with the accreting matter onto the black hole. Such a state is the so-called slim accretion disk [50]. Clearly, in order to understand accretion physics in these systems, radiation MHD models with self-consistently coupled gas, radiation, and magnetic fields are important.

In this short review, I will overview the recent progress in the study of relativistic jet formation via GRMHD simulations and the modeling of relativistic jets based on the results of GRMHD simulations. In Section 2, I discuss jet formation from geometrically thin accretion disks. Jet formation from geometrically thick accretion torii is discussed in Section 3. I then present an overview of radiative GRMHD simulations and the effects on jet formation in Section 4. I briefly touch on some GRMHD simulations for jet formation without accretion disks in Section 5. Then, in Section 6, I discuss jet modeling work using the results of GRMHD simulations. Finally, I summarize the current progress and findings in Section 7.

2. Jet Formation from Geometrically Thin Accretion Disk

Pioneering work of relativistic jet formation via GRMHD simulations was performed by Koide et al. [51,52] in the consideration of a Keplerian thin accretion disk with a strong vertical magnetic field around a non-rotating black hole. In these two-dimensional (2D) simulations, the matter in the disk loses angular momentum by magnetic breaking and then falls into the black hole. A centrifugal barrier near the black hole horizon decelerates the infalling material and produces a standing shock. Plasma near the shock is accelerated by the Lorentz force and forms bipolar jets. Inside these magnetically driven jets, the gradient of gas pressure also generates a jet above the shock region (gas-pressure-driven jets). Such two-layered jets are formed in both a hydrostatic corona and a radially infalling corona. Koide et al. [10] extended this work to rotating black holes and found that similar two-layered jets are produced in both co-rotating and counter-rotating black hole magnetospheres. This simulation was extended to three dimensions (3D) by Nishikawa et al. [53].

After this, Hardee et al. [54] performed similar GRMHD simulations of Keplerian thin disks with vertical magnetic fields, now considering different black hole spins. In this study, the formation of two-component jets due to black hole spin effect is demonstrated. The resulting jet is mildly relativistic ($\sim 0.5c$). Due to numerical limitations, these earlier simulations did not investigate the long-term evolution.

Thin disk simulations have been used for the investigation of the validity of Novikov and Thorne disk theory [48], finding around a 10% deviation of radiative efficiency (e.g., [55–58]). In much stronger magnetic field cases, such as magnetically arrested disk states, such deviations becomes much larger, reaching up to ∼80% [59]. Recently, Dihingia et al. [60] has shown the formation of a BZ-jet from a black hole and BP disk wind from a thin accretion disk with an inclined poloidal magnetic field geometry (see Figure 1). These authors also found that plasmoids are formed in thin accretion disks due to magnetic reconnection. Near the polar axis, there are strong magnetized regions in which the BZ process operates and can launch jets. The jet velocity can reach around $\gamma \sim 10$. This result indicates that strong initial poloidal magnetic fields are essential for creating strong jet and disk winds from thin accretion disks.

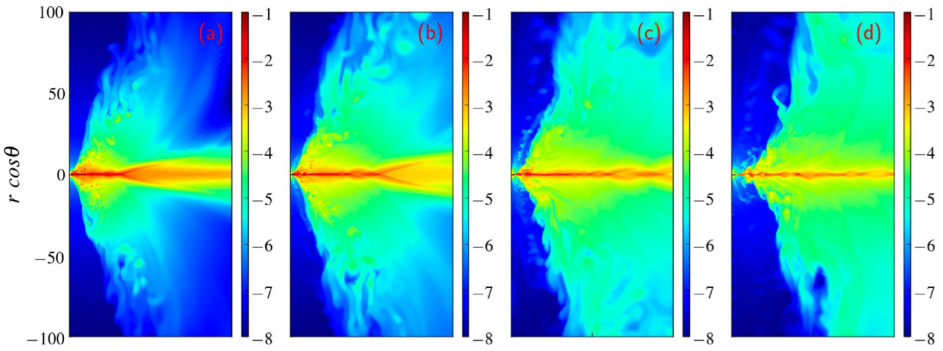

Figure 1. Evolution of 2D GRMHD simulations of a geometrically thin disk around a rotating black hole at $t = 500$ (**a**), $t = 1000$ (**b**), $t = 2000$ (**c**), and $t = 4000$ (**d**). The color contour is logarithmic normalized density ($\rho/\rho_{\rm max}$). Figure is reproduced with permission from Dihingia et al. MNRAS, 505, 3596 (2021) [60].

2.1. Jet Formation from Tilted Thin Disks

The misalignment between the accretion disk and the black hole angular momentum vector is another degree of freedom of GRMHD simulations. Important changes in the dynamics of an accreting system exhibiting such misalignment are thought to be a result of Lense–Thirring (LT; Lense and Thirring, 1918) precession. LT precession is a general relativistic frame dragging effect where test particles on tilted orbits around the central object precess with a radially dependent angular frequency $\Omega_{\rm LT} \propto 1/r^3$. Bardeen and Petterson [61] showed that a viscous disk would be expected to relax to a configuration where the inner region becomes aligned with the equatorial plane of the

black hole. Liska et al. [62] have investigated the Bardeen–Petterson alignment using high-resolution GRMHD simulations with thin accretion disks, showing the alignment in the inner region of the disk (see Figure 2). They have also demonstrated that powerful relativistic jets are still launched in this misaligned case. Interestingly, in the case of highly tilted disks, the disk is torn apart and forms a rapidly precessing inner sub-disk with a slowly precessing outer sub-disk [63]. The resulting jet precesses rapidly together with the inner sub-disk.

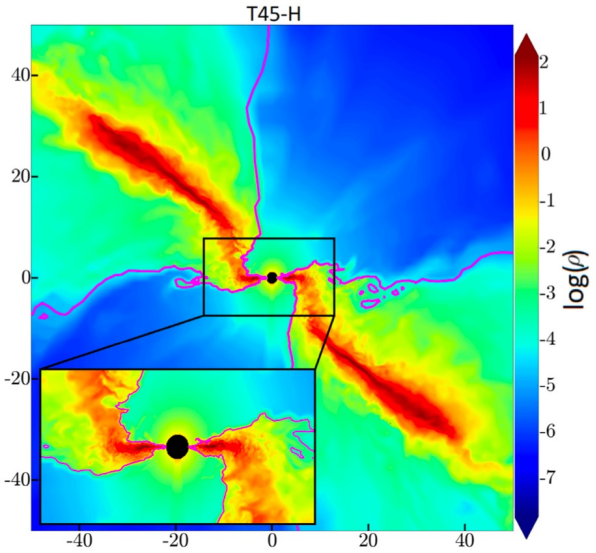

Figure 2. Snapshot of a vertical slice from a 3D GRMHD simulation of a tilted thin disk. The color contour shows logarithmic density. Magenta lines indicate the jet boundary, defined as $p_b = 5\rho c^2$. The results present the alignment of the inner disk along the equator. Figure is reproduced with permission from Liska et al. MNRAS, 507, 983 (2021) [63].

2.2. Thin Disk Simulations in Non-Ideal GRMHD

GRMHD simulations of jet launching from thin accretion disks have been extended to the non-ideal regime by including resistivity [64,65]. It was found that magnetic diffusivity lowers the efficiency of accretion and ejection. The launched jet and wind become weaker and slower ($\simeq 0.1c$).

In general, radiation effects are an important property in modeling thin accretion disks, in particular, radiative cooling. However, most GRMHD simulations of thin accretion disks do not include such effects due to the numerical difficulty and computational cost. Therefore, in order to obtain a more realistic picture of jet formation from thin accretion disks, radiation GRMHD simulations need to be performed.

3. Jet Formation from Geometrically Thick Magnetized Torii

Modern BH accretion disk theory suggests that angular momentum transport is provided by Maxwell and Reynolds stresses within the orbiting plasma. MHD turbulence is driven by the magnetorotational instability (MRI) within a differentially rotating disk [66,67]. Convective motions developed by MRI are a general phenomenon in RIAFs. Since the viscosity that drives accretion originates from MRI, magnetic fields play a crucial role. In order to develop MRI in the accretion disk, in general, a geometrically thick accretion torus with a weak poloidal magnetic loop inside the torus is considered. The disk thickness (H/r, where H is height of the disk and r is the radius from a black hole) is a key parameter for capturing the MRI in numerical simulations. If H/r becomes smaller, much greater numerical resolution is needed to resolve the accretion disk. Therefore, geometrically thick torii are favored as the initial setup for numerical simulations.

Pioneering GRMHD simulations of thick accretion torii in RIAFs were performed by De Villiers and Hawley [68] and McKinney and Gammie [69]. De Villiers and Hawley [68]

studied the accretion process in rotating black hole spacetimes and investigated the dependency of the accretion on the black hole spin parameter. McKinney and Gammie [69] estimated the outward energy flux from the Kerr black hole horizon via the BZ process. In their simulations, a flow structure can be decomposed into a disk, a corona, a disk wind, and a highly magnetized polar funnel (see Figure 3) (e.g., [70,71]). Such an accretion flow regime is termed standard accretion and normal evolution (SANE). RIAFs with poloidal magnetic flux and a spinning black hole are key ingredients for producing Poynting-flux-dominated (PFD) funnel jets (e.g., [12,69,70,72–76]). Between the PFD polar funnel jet and the disk wind, there is the region of unbound mass flux referred to as the "funnel-wall" jet. The boundary between the low-density PFD funnel jet and the high-density funnel wall jet is sharp and clear. The properties of the disk wind have been investigated for different black hole spins and magnetic field configurations (e.g., [77,78]).

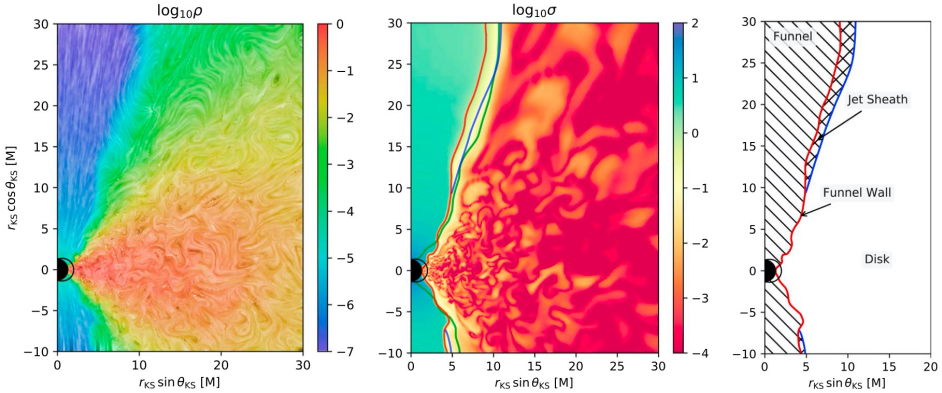

Figure 3. Snapshot of GRMHD simulations of geometrically a thick torus in the SANE regime. Left: color contour shows logarithmic density and white lines indicate rendering of the magnetic field structure using line-integral convolution. Center: color contour shows logarithmic magnetization. The magnetized funnel is represented by $\sigma = 1$ (red lines), the disk is indicated by $\beta = 1$ (green lines), and the geometric Bernoulli criterion ($u_t = -1$) is given by the blue solid line in the region outside of the funnel. Right: schematic of the main components of SANE regime. Figure is reproduced with permission from Porth et al. ApJS, 243, 26 (2019) [79].

From theoretical work on jets (outflows), jet structure is understood to depend on the interaction of outflows with the ambient medium. Understanding the coupling between outflows and ambient medium requires information about the magnetic field configuration, physical conditions at the jet base, and the properties of the ambient medium, because these are related to the jet's final energy contents and Lorentz factor. Many idealized semi-analytic studies have been performed to investigate jet properties (e.g., [80–83]).

Comparison of GRMHD simulations with steady solutions of force-free jets have shown good agreement of these properties with the PFD funnel jet (e.g., [84,85]). PFD jet profiles in time-averaged GRMHD simulations exhibit a power-law profile to the parabolic solution. This is similar to the solution of Blandford and Payne [5]. McKinney and Narayan [86] confirmed that similar profiles are obtained from general relativistic force-free electrodynamics simulations of the disk wind.

However, there semi-analytic models and GRMHD simulations disagree in the characteristics of jet acceleration. Semi-analytic models (e.g., [81]) have reported efficient acceleration of jets to nearly the maximum Lorentz factor by converting the jet's entire energy budget. Such results are confirmed by global SRMHD simulations of jets injected from a disk with the ambient medium modeled by placing a conducting wall at the jet outer boundary (e.g., [87–90]), which shows bulk acceleration up to $\gamma_\infty \sim$ 10–1000. However, such highly efficient energy conversion is not seen in GRMHD simulations (e.g., [70]). In McKinney [70], the simulations are extended up to $r = 10^4$ M and show $\gamma_\infty \leq 10$. Acceleration is saturated beyond a few times 100 M. Recently, Chatterjee et al. [91] has extended the investigation of jet acceleration up to 10^5 M in axisymmetric (i.e., 2D) GRMHD

simulations. They found the development of oscillations by the interaction between jet and wind. Such oscillations drive pinch instabilities at the jet outer boundary when the jet becomes superfast (see [70]). These pinch instabilities result in a heating up of the jet by magnetic reconnection and mass loading of the jets which affects the jet deceleration. Such pinch modes may excite kink instabilities in 3D configurations.

When jets are magnetically dominated, they are likely to experience current-driven kink instabilities, which will lead to magnetic reconnection (e.g., [92–98]). A kink instability excites large-scale helical motions that may disrupt the regular structure of the magnetic field, liberating magnetic energy and potentially resulting in flaring activity like that observed from blazars (e.g., [99]). Such magnetic reconnection driven by kink instability-induced turbulence may be a possible mechanism for rapid magnetic dissipation of relativistic jets and high-energy particle acceleration (e.g., [100]).

Global SRMHD simulations of jet injection and propagation in the ambient medium have shown bulk jet acceleration to occur (e.g., [88,90]). When such external pressure support drops and the jet enters the the regime of ballistic expansion, additional acceleration occurs via magnetosonic rarefaction waves from the boundary between the jet and the ambient medium. This is the so-called rarefaction acceleration, which induces a conversion of magnetic energy into kinetic energy of the bulk motion (e.g., [7,8,101,102]). Such wave propagation in relativistic jets produces multiple chains of expansion and recollimation, with shocks and rarefaction waves (e.g., [103]). Standing recollimation shocks in relativistic jets are related to stationary features observed in relativistic jets [104].

Recently, GRMHD simulations of magnetized accretion torii around black holes in an alternative theory of gravity (dilaton black hole in Einstein–Maxwell dilaton–axion theory of gravity), and even exotic compact objects like a boson star, have been performed [105,106]. Although they have currently applied only to spherically symmetric black holes and exotic compact objects, these simulations are useful for understand the dynamics and testing theories of gravity from the accreting matter, as well as understanding jet formation in the different theories of gravity.

GRMHD simulations of magnetized accretion torii in the SANE regime are a standard model for GRMHD simulations. Porth et al. [79] performed a code comparison of many existing GRMHD codes, using the same initial setups in the SANE state. In this code comparison challenge, nine GRMHD codes participated, with the results showing that agreement between GRMHD codes improves as resolution increases, obtaining consistent results.

3.1. GRMHD Simulations in the MAD Regime

One of the key properties of an accretion flow is the magnetic field, and it is particularly important to understand the accretion flow behavior in the magnetically dominated regime. Igumenshchev et al. [107] found that magnetic fields can become dynamically important in black hole accretion flows, preventing the inward motion of the accretion flow via magnetic pressure near the horizon (see Figure 4) (e.g., [108]). This regime is called the magnetically arrested disk (MAD) (e.g., [109]). Hot accretion flows in the MAD regime can produce powerful jets (e.g., [110–112]). White et al. [113] have studied the effects of numerical resolution on dynamical properties in the MAD state and demonstrated convergence. Recently, Narayan et al. [114] investigated black hole spin dependency in the MAD state by considering the long-term evolution of GRMHD simulations. They found that the saturated magnetic flux level and jet power in the MAD regime depend strongly on the black hole spin. The prograde spin case saturates at much higher relative magnetic flux and has more powerful jets than in retrograde cases. Similar trends are seen in Tchekhovskoy and McKinney [110]. MAD simulations with spinning black holes have launched powerful jets with generalized parabolic profiles which follow the width $w \propto z^k$, where z is jet height and power law index $k \sim 0.27$–0.42 from the range of height $z = 5$–$100\, r_g$, and $r_g \equiv GM/c^2$ is gravitational radius. This is similar to jets in the SANE case. The jet width also depends

on the black hole spin. Prograde cases show wider jets compared to retrograde cases. Even in jet images at mm wavelengths, similar results in jet width are seen [115].

GRMHD simulations in the MAD regime exhibit violent episodes of flux escape from the black hole magnetosphere (e.g., [116,117]). These magnetic flux eruptions could explain the flare events observed in Sgr A* because they are associated with magnetic reconnection, which provides particle heating and acceleration during the flare events and contains enough energy to power flares. Wong et al. [118] have investigated the jet–disk boundary layer in different black hole spins and different accretion states, including SANE and MAD. They have shown that in the retrograde case, due to strong shear, the jet–disk boundary is unstable. This mixing layer episodically loads matter onto trapped field lines where it is forced to co-rotate with the BH, and move outward into the jet.

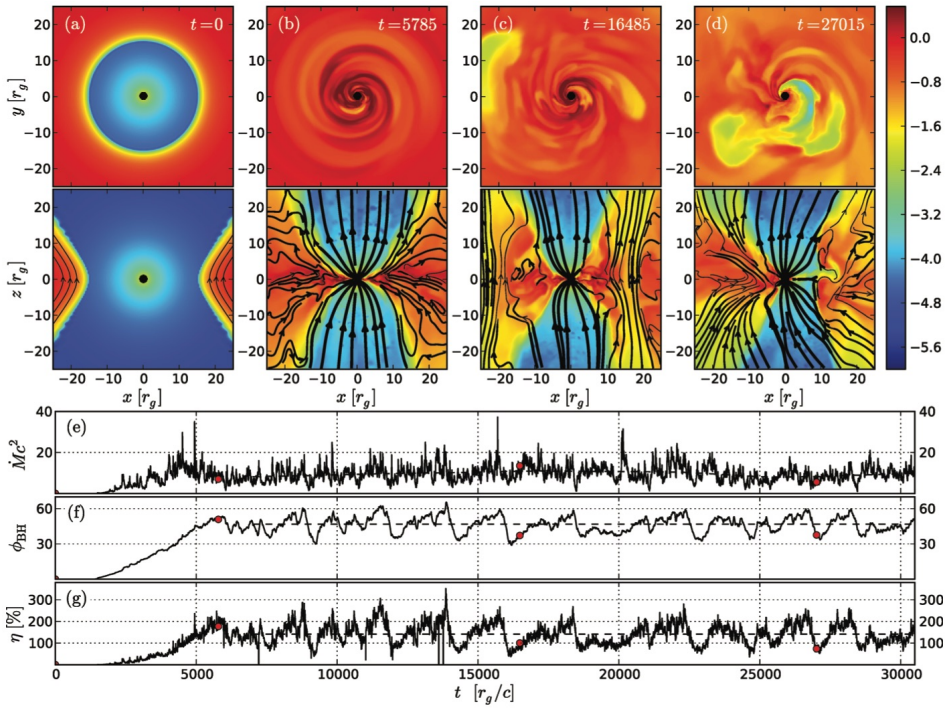

Figure 4. Snapshot of GRMHD simulations of a geometrically thick torus in the MAD regime (Panels (**a**–**d**)). The top and bottom rows show equatorial ($z = 0$) and vertical ($y = 0$) snapshots of the simulation. Color represents logarithmic density and black lines indicate magnetic field lines. Panels (**e**–**g**) show the time evolution of the mass accretion rate, magnetic flux threading the BH horizon, and the energy outflow efficiency. Figure is reproduced with permission from Tchekhovskoy et al. MNRAS, 418, L79 (2011) [112].

Recent polarized observations of M87 by the Event Horizon Telescope indicate that the accretion flows in M87 will be in the MAD state [119]. Other discussions of observed jet power in AGNs also suggest that MAD is favored in those systems [120,121].

3.2. Different Magnetic Field Configurations

Magnetic field configuration is another important ingredient of accretion flows which result in jet production. In standard GRMHD simulations of magnetized accretion torii, single poloidal magnetic loops inside the torus are considered and result in stationary jet formation (e.g., [12,70,73,79]). In general, different poloidal magnetic field configurations result in different magnetic flux accretions onto the black hole horizon and jet launching properties (e.g., [76,77,111,122–124]). In particular, the configuration of multiple poloidal magnetic loops with different polarities leads to intermittent, non-stationary jet formation (e.g., [125,126]). In same-polarity multiple poloidal magnetic loop cases, same-polarity loops quickly reconnect to form a large loop with a resulting flow similar

to the single magnetic loop case. On the other hand, opposite-polarity loops preserve their small coherence length. This generates plasmoids and plasmoid chains by magnetic reconnection, which results in flaring activity. Similar plasmoid formation has even been seen in single poloidal loop cases at the jet funnel wall region in general relativistic resistive MHD simulations [127]. If GRMHD simulations with multiple loops enter a MAD regime, plasmoid chains develop on the equatorial plane near the horizon and a quasi-striped jet is produced [128]. In long-term evolution, jets become inactive and the accretion flow state transitions to the SANE regime. In general, GRMHD simulations with multiple magnetic loops need higher numerical resolution to resolve plasmoid formation and the development of plasmoid chains. At present, most of these simulations are performed in 2D. Therefore, it is important to investigate how plasmoids and intermittent jets develop in 3D GRMHD simulations.

In the general consensus of jet formation via MHD processes, one requires poloidal magnetic fields, hence many GRMHD simulations are performed with poloidal magnetic fields in order to produce relativistic jets. Large-scale poloidal magnetic fields can be formed in situ through a turbulent dynamo [129] produced by the MRI. In earlier studies, Beckwith et al. [76] presented jets that cannot be formed from a purely toroidal magnetic field initial condition. In larger torus configurations, McKinney et al. [111] found that weak jets can form from toroidal magnetic field initial configurations. Recently, Liska et al. [130] showed that a simulation with a toroidal magnetic field can generate poloidal fields self-consistently via an α dynamo and produce relativistic jets. From these simulations, it has been learned that numerical resolution is important. High numerical resolutions are needed to capture turbulent dynamo processes seen in local shearing box simulations.

Toroidal magnetic field configurations in geometrically thick torii are used to investigate the stability of the system. Komissarov [131] described a new torus solution with purely toroidal magnetic fields. If this torus solution is strongly magnetized, the system is unstable to non-axisymmetric MRI [132] and over a few tens of orbital periods, the magnetization of the disk significantly drops before reaching its steady-state value in the weakly magnetized disk [133]. Bugli et al. [134] have studied the effect of the Papaloizou–Pringle instability for a thick torus with a toroidal magnetic field, finding that weak toroidal magnetic fields suppress the development of the Papaloizou–Pringle instability.

3.3. Jet Formation from Tilted Thick Torii

As discussed in the previous section, misalignment (tilt) between the accretion disk and black hole spin axis brings in another free parameter for jet formation simulations of magnetized torii. The first GRMHD simulations with a tilted torus were performed by Fragile et al. [135]. Tilted disk configurations present more complicated dynamics than untilted systems. In such simulations, the main body of the disk remains tilted and there is no indication of a Bardeen–Petterson effect in the disk at large. When the tilt angle becomes large, the tilted disk can develop standing shocks that can facilitate the transport of angular momentum and dissipation of energy in the disk [136]. Recently, White et al. [137] performed a parameter survey of tilted torii with different black hole spin parameters and inclination angles. In their simulations, magnetized polar outflows form along the disk rotation axis, in agreement with Liska et al. [62] for tilted thin disk simulations (see Figure 5). Similar results are also obtained by Chatterjee et al. [138]. A parameter study by White et al. [137] confirmed the presence of standing shocks at large inclination angles and no observable Bardeen–Petterson effect. Many GRMHD simulations suggest that tilted torus simulations can produce relativistic jets as seen in non-tilted torus simulations. However, the jet propagation direction is still not fully understood. The jet propagation direction will affect the interpretation of black hole shadow images, since the inferred observer inclination angle depends on the jet orientation in the sky.

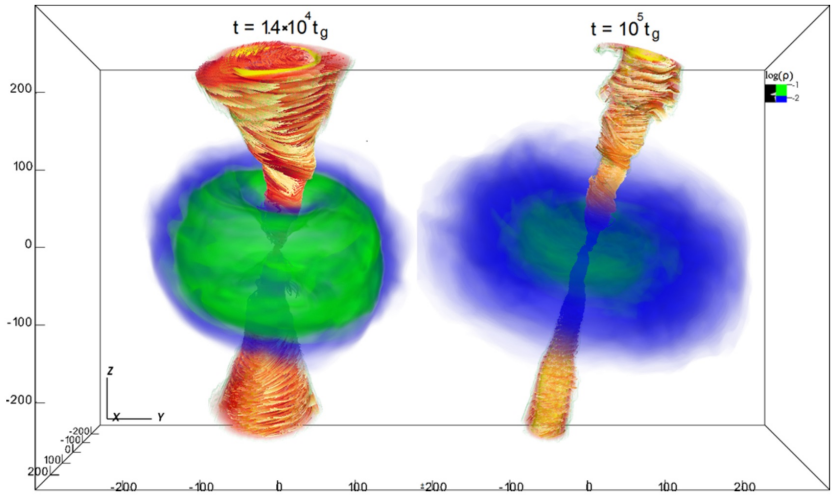

Figure 5. 3D volume rendering of density (green and blue) and jet magnetic field colored by magnetic energy (red and yellow) in GRMHD simulations of a tilted torus. Figure is reproduced with permission from Liska et al. MNRAS, 474, L81 (2018) [62].

3.4. Geometrically Thick Torus Simulations in Non-Ideal GRMHD

In RIAFs, the Coulomb mean free paths of both ions and electrons are much larger than the typical length scale of disks, $\sim r_g$ [139]. Therefore, the plasma in the disks is expected to be collisionless. This raises questions about the validity of the ideal MHD approximation in RIAFs. One extension of ideal MHD approaches is the so-called weakly collisional plasma model. In this approach, non-ideal effects are treated as perturbations relative to an ideal fluid. This includes anisotropic heat and momentum transport. Chandra et al. [35] have described a covariant form for a weakly collisional magnetized plasma and developed a new extended GRMHD code [36]. Application to the accretion torus in RIAFs has been performed by Foucart et al. [140,141]. They found that pressure anisotropy produces outward angular momentum transport with a magnitude comparable to that of MHD turbulence in the disk, along with a significant increase in temperature at the funnel wall region. They also found that the heat flux is dynamically unimportant. These simulations in extended GRMHD have shown similarities to those in ideal GRMHD simulations. Therefore, accretion flows neglecting non-ideal effects are likely reasonable even if the accretion flows are nearly collisionless.

Another extension from ideal MHD is adding resistivity. In ideal GRMHD simulations of magnetized accretion flows, dissipation is seen at the grid scale due to numerical resistivity (e.g., [125]). To study magnetic reconnection and plasmoid formation, it is therefore better to consider reconnection physically. Recently, Ripperda et al. [38] developed a resistive GRMHD simulation code. In that simulation, an explicit finite resistivity acts as a proxy for kinetic effects, presenting a physical model of magnetic reconnection and plasmoid formation in turbulent black hole accretion flows [127]. Tomei et al. [142] have investigated a mean-field dynamo in resistive GRMHD simulations of a magnetized accretion torus in the full non-linear regime. The dynamo process produces an exponential growth of initial seed magnetic field [143]. Different dynamo coefficients provide different growth rates, although the magnetic field amplification seems to saturate at similar levels. Resistive GRMHD simulations have similar difficulties to radiation GRMHD, because the resistive term provides a stiffness in the equations. Therefore, the stiff term needs to be solved implicitly.

4. Jet Formation in Radiative GRMHD Simulations

GRMHD simulations of jet launching have been performed from magnetized thick accretion torii for RIAFs. In accretion theory, depending on the mass accretion rate, radiation

effects become important near the Eddington limit. When considering accretion flows with mass accretion rates close to the Eddington limit, a proper treatment of radiation is crucial.

One rather simple treatment of radiation is through considering radiative cooling. A simple local cooling prescription via different radiation processes is implemented in GRMHD codes (e.g., [144–146]). Dibi et al. [145] have identified that even for mass accretion rates of $\dot{M}/\dot{M}_{\rm Edd} \approx 10^{-7}$, radiative losses may play an important role in GRMHD simulations, where $\dot{M}_{\rm Edd}$ is the Eddington mass accretion rate.

Another approach for radiative cooling is using a full frequency- and angle-dependent Monte Carlo treatment of the radiation field [147–150], coupled with GRMHD simulations. These have been applied to simulations of RIAFs, obtaining similar results and concluding that global radiative effects play a sub-dominant yet non-negligible role in disk dynamics if $\dot{M}/\dot{M}_{\rm Edd} \geq 10^{-6}$, as suggested by Dibi et al. [145].

Full coupling with radiation in GRMHD simulations is challenging due to the stiffness of the radiative term. Farris et al. [151] developed a formalism for incorporating radiation in the Eddington approximation (flux-limited diffusion approximation). Such formalisms have been implemented in several GRMHD codes [152]. However, the Eddington approximation cannot handle optically thin flows accurately. More advanced methods have since been developed (e.g., [30,31]). These methods solve the radiation momentum equations using an M1 closure scheme. They perform GRRMHD (the second "R" denoting "radiative") simulations of super-critical accretion disks (e.g., [153–156]). These simulations have shown that even super-Eddington accretion disks around spinning black holes produce low-density funnels, with large fractions of energy being extracted from the black hole's rotational energy through a process similar to the BZ mechanism (see Figure 6). Importantly, these simulated systems have a high radiative efficiency which significantly exceeds the efficiency predicted by slim disk models for these mass accretion rates. The magnetized jet creates a low-density channel for radiation and pushes away the more opaque wind. This leads to radiation flux escaping from the disk and reduces the conversion of radiation energy flux into kinetic energy flux of the wind. Such a mechanism enables high radiative efficiencies in supper-Eddington accretion flows.

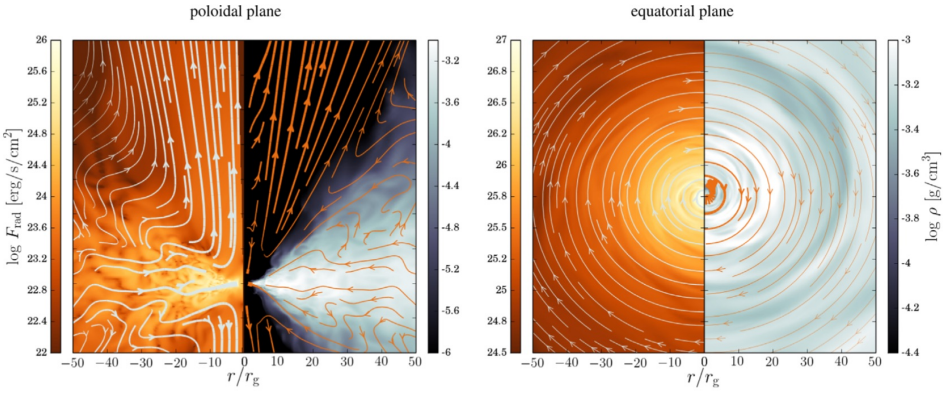

Figure 6. Snapshot images of radiative flux (left half of each panel) and density (right half of each panel) in the radiation GRMHD simulations of a thick torus. The left and right panels correspond to vertical and equatorial slices, respectively. Lines indicate azimuth- and time-averaged radiative flux and gas velocity. Figure is reproduced with permission from Sadowski and Narayan, MNRAS, 456, 3929 (2016) [156].

5. Jet Formation without Disk

In general setups for the simulation of jet formation, there is a hydrostatic equilibrium of the thin disk or thick torus with the poloidal magnetic field surrounding the central black hole (e.g., [79]). One general question which is raised is whether an accretion disk or a torus is required for jet formation. If the accreting matter has angular momentum, matter piles up on the equatorial plane and creates a disk-like structure. If this accreting matter involves poloidal magnetic fields, jet-like outflows develop from the resulting disk-like structure

via ordinary MHD processes (e.g., [157,158]). Garain et al. [159] performed GRMHD simulations of poloidal magnetic fields advected within low angular momentum accretion flows, yielding outflows from the centrifugal barrier near the horizon. Even GRMHD simulations of spherical accretion flows with magnetic fields have been investigated [160]. Though the advection of uniform, relatively weak magnetic fields and a spinning black hole, magnetic reconnection-driven turbulence develops on the equatorial plane, nearly reaching the MAD state and forming electromagnetic jets in the polar region. A jet is formed even when there is no initial net vertical magnetic flux, since turbulent, horizon-scale fluctuations can generate a net vertical magnetic field locally.

Ressler et al. [161] considered a more realistic situation in Sgr A* and performed GRMHD simulations of accretion flows fed by ∼30 Wolf–Rayet (WR) stellar winds. The initial conditions of these simulations were provided by larger-scale MHD simulations [162]. WR stellar winds provide weak magnetic field at large scales. These are amplified by flux freezing and compression within the inflowing gas before reaching the horizon. The accretion flow enters the MAD state through continuous accretion of coherent magnetic fields. The amplified magnetic field then helps to drive polar outflows.

Several GRMHD simulations have shown that accretion disks or torii are not initially required for jet formation. The jets which form in these simulations are not persistent in some cases. An outstanding issue is the investigation of the similarities and differences between accretion and outflow dynamics in different physical conditions. This will help establish the critical requirements for jet formation.

6. Jet Modeling from GRMHD Simulations

When matter accretes onto a black hole, it heats up and begins to radiate. Since the radiation within the black hole photon orbit falls into the horizon and never reaches us, the presence of the horizon casts a "shadow". In GR, the size of this shadow only depends on the mass and spin of the black hole. Therefore, the direct observation of a black hole is a very promising approach to investigate the properties of a black hole and its surrounding plasma dynamics, including the accretion flow and the formation of jets (e.g., [163–165]).

General relativistic radiative transfer (GRRT) calculations coupled with the calculation of geodesics in the black hole spacetime are an essential tool for determining the images, spectra, and light curves from matter in the vicinity of BHs. Without scattering, the integration of the radiation transfer equation can be performed by dividing each ray into a series of small steps. This is the so-called ray-tracing method. Several GRRT codes have been developed to utilize this ray-tracing method (e.g., [166–177]). Some of these GRRT codes are coupled with GRMHD simulation codes to produce observables such as images, spectra, light curves, and polarization.

The horizon scale image of a black hole accretion system is closely related to the origin of jets and their structure. The horizon scale image at mm/sub-mm wavelengths for M87 was first discussed in Broderick and Loeb [178]. In order to model the jet structure, Broderick and Loeb [178] assumed a force-free jet model and plasma loading at a certain height above the horizon. A modified version of the jet model, taking into account the jet terminal Lorentz factor, was considered in Lu et al. [179]. How different background jet velocities result in different shearing hot spot features within the jet and disk wind is discussed in Jeter et al. [180]. Takahashi et al. [181] investigated the large-scale jet image feature for different plasma loadings at the foot point of the jet. In a GRMHD flow, there is a region close to the black hole inside of which matter is accreted and outside of which the matter is accelerated outward. This is the so-called stagnation surface, which is defined by a vanishing poloidal velocity. Such a region is theoretically predicted to be highly magnetized and exhibit low densities, providing an ideal site for energetic, non-thermal, and non-ideal processes. Provided that energetic electrons could be injected from the stagnation surface, Pu et al. [182] have considered the subsequent plasma cooling coupled with a GRMHD background velocity, and proposed that the emission from this stagnation surface could be an observable feature if the jet launching mechanism originates from GRMHD processes.

Calculating the emission from accreting matter requires predicting the electron distribution function. In a thermal synchrotron radiation model, a Maxwell–Jüttner distribution function with a particular electron temperature is assumed. In an RIAF, asymmetric heating and inefficient Coulomb coupling between electrons and protons lead to a decoupling of electron and proton temperatures. Most GRMHD simulations only consider a single fluid, which essentially describes the ions (mass, temperature, and energy). Therefore, the emitting electron temperature is not constrained. In order to overcome this issue, typically, the electron-to-ion temperature ratio is prescribed manually in post-processing GRRT calculations of GRMHD simulations (e.g., [183–188]). The standard prescription for the electron temperature assumes a constant fraction of the ion temperature (e.g., [185,187,189]). In many cases, the emitting region can be broken down into components according to different physical properties, such as the disk and the jet/funnel. Mościbrodzka et al. [186] proposed a parametrized electron-to-ion temperature ratio formula which follows the plasma beta distribution of GRMHD simulations. This is the so-called R-β prescription. This temperature prescription leads to a hotter electron temperature within more magnetized regions, i.e., jet regions, helping to produce the observed flat radio spectra and making the jet more prominent compared to the accretion disk. Other parametrized prescriptions for the electron temperature are proposed in other studies [183,188,190,191] which are based on energy balance arguments and the properties at larger radii. Models inspired by the results of electron thermodynamics in GRMHD simulations have also been considered in recent years (e.g., [192,193]). The first model of M87 based on GRMHD simulations was presented by Dexter et al. [184]. Their models included a thermal electron population in the disk and a power-law-based electron distribution in the jet. Mościbrodzka et al. [186] reproduced the characteristics of the M87 radio core, namely a flat spectrum and an increasing image size with observing wavelength, by adopting a two-temperature accretion flow with a hot isothermal jet.

A more self-consistent approach for obtaining electron temperature from GRMHD simulations involves coupling with electron thermodynamics, where one evolves an electron entropy equation which takes into account local sub-grid electron heating [116,147,149,192–195]. In this approach, the back reaction of electron pressure on the dynamics of the accretion flow is neglected (see [192]). For the electron heating prescription, this study used two major heating models, turbulent heating (e.g., [196,197]) and magnetic reconnection heating (e.g., [198,199]). Mizuno et al. [193] confirmed that the commonly used parametrized electron-to-ion temperature ratio prescription R-β model is well matched to both turbulent and magnetic reconnection electron heating models, when comparing with images at 230 GHz. Recently, two-temperature radiation GRMHD simulations have been performed for M87, taking into account the dynamical importance of the photon field on the accretion structure as well as electron cooling [149,194]. In particular, Chael et al. [194] have found that MAD GRMHD simulations with high BH spin produce wide opening angle jets consistent with VLBI images at 43 and 86 GHz (see Figure 7). Similar results are found from MAD GRMHD simulations using a hybrid electron distribution function [115,200].

One of the major open questions in modeling the electromagnetic radiation emerging from accretion flows and jets is the shape of the electron distribution function (eDF). The common assumption is that the electrons in the full simulation domain are in a thermal-relativistic Maxwell–Jüttner distribution. However, this assumption likely breaks down in regions where non-ideal MHD effects are important.

Davelaar et al. [201] applied the κ-eDF in jet regions of axisymmetric 2D GRMHD simulations. The κ-distribution function is a combination of a relativistic thermal and a relativistic non-thermal power-law distribution, and describes accelerated electrons (e.g., [202–205]). They found that κ-jet models increase the radio-emitting region size and radio flux for decreasing values of the κ parameter, which corresponds to a larger amount of accelerated electrons in the jet region. In Davelaar et al. [206], this work is extended to using 3D GRMHD simulations and a variable κ model which is based on sub-grid particle-in-cell (PIC) simulations of trans-relativistic magnetic reconnection [207]. This result shows that

κ-eDF models reproduce the broad band spectrum from radio to optical wavelengths of M87, which cannot be produced from thermal eDFs. Recently, Cruz-Osorio et al. [200] investigated the impact of a non-thermal emission models on the structure and morphology of the M87 jet and its spectrum by using MAD GRMHD simulations. They found that MAD models can explain both the observed jet width of M87 at 86 ĜHz (e.g., [208]) and its spectrum.

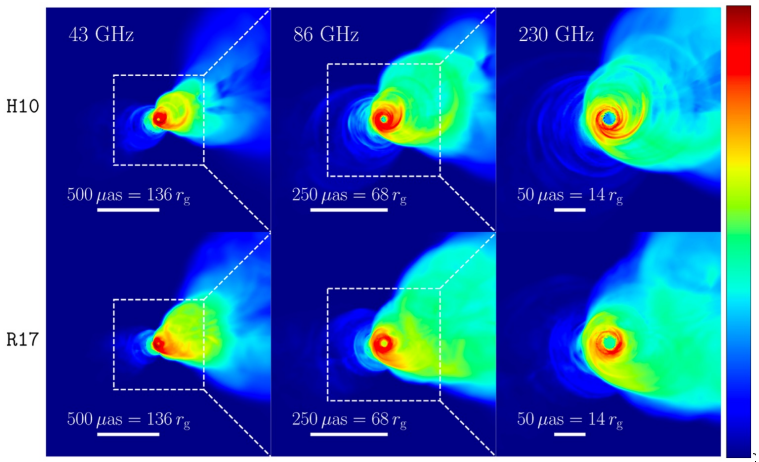

Figure 7. Logarithmic scale radiation images of two-temperature GRMHD simulations of a MAD torus with electron heating prescription at 43 ĜHz (**left**), 86 ĜHz (**middle**), and 230 ĜHz (**right**). Snapshots were observed at an inclination angle of 17 degrees with respect to the simulation south pole and rotated 108 degrees counterclockwise, in order to fit the observed jet orientation. Figure is reproduced with permission from Chael et al. MNRAS, 486, 2873 (2019) [194].

Current modeling studies based on GRMHD simulations are dominated by RIAFs. Jets in low-luminosity AGNs, in particular M87, have been observed from Mpc scales to sub-pc scales in high structural detail. There is strong motivation to model such jets and extract fundamental physics. Recent GRMHD simulations have been extended to more varied setups, including thin disks and slim disks. GRRT calculations coupled with these GRMHD simulations will provide jet modeling in a wide variety of AGN jets.

7. Discussion and Summary

Over the past few decades, many GRMHD codes have been developed and applied to study relativistic jet formation in various physical conditions, from geometrically thin disks to geometrically thick torii, with additional physical processes such as radiation feedback. It is understood that poloidal magnetic fields near the black hole horizon are a key ingredient required to produce powerful relativistic jets via MHD processes. Relativistic jets are accelerated around a Lorentz factor of less than 100. However, for further acceleration, additional magnetic energy dissipation mechanisms are required.

Recent progress from GRMHD codes using AMR and including different physics such as resistivity and radiation have provided a much wider variety of dynamics of accretion flows onto black holes and corresponding jet formation. This growing diversity in modeling will be important for the fundamental understanding of accretion and jet physics.

From the recent progress of millimeter and sub-millimeter VLBI observations from observatories such as the EHT and GMVA, the collimation and acceleration zones of relativistic jets in several AGNs could be observed. Theoretical modeling of relativistic jets from GRMHD simulations is hence becoming increasingly important. GRMHD simulations of jet formation and subsequent modeling will play a crucial role in the understanding of relativistic jet properties, including jet formation and acceleration mechanisms, which may all be investigated via comparison with future mm- and sub-mm VLBI observations.

Funding: This research is supported by the ERC synergy grant 'BlackHoleCam: Imaging the Event Horizon of Black Holes' (grant number 610058).

Data Availability Statement: The data underlying this article will be shared on reasonable request to the corresponding author.

Acknowledgments: I would like to thank Ziri Younsi for useful discussions. This research has made use of NASA's astrophysics data system (ADS).

Conflicts of Interest: The author declares no conflict of interest.

Abbreviations

The following abbreviations are used in this manuscript:

ADAF	Advection-Dominated Accretion Flow
AGN	Active Galactic Nuclei
AMR	Adaptive Mesh Refinement
BH	Black Hole
EHTC	Event Horizon Telescope Collaboration
GR	General Relativity
GRMHD	General Relativistic Magnetohydrodynamics
GRRT	General Relativistic Radiative Transfer
MAD	Magnetically Arrested Disk
MHD	Magnetohydrodynamics
MRI	Magnetorotational Instability
SANE	Standard Accretion and Normal Evolution
PFD	Poynting Flux Dominated
RIAF	Radiatively Inefficient Accretion Flow
WR	Wolf–Rayet

References

1. Begelman, M.C.; Blandford, R.D.; Rees, M.J. Theory of extragalactic radio sources. *Rev. Mod. Phys.* **1984**, *56*, 255–351. [CrossRef]
2. de Gouveia Dal Pino, E.M. Astrophysical jets and outflows. *Adv. Space Res.* **2005**, *35*, 908–924. [CrossRef]
3. Beskin, V.S. Magnetohydrodynamic models of astrophysical jets. *Phys. Uspekhi* **2010**, *53*, 1199–1233. [CrossRef]
4. Blandford, R.D.; Znajek, R.L. Electromagnetic extraction of energy from Kerr black holes. *Mon. Not. R. Astron. Soc.* **1977**, *179*, 433–456. [CrossRef]
5. Blandford, R.D.; Payne, D.G. Hydromagnetic flows from accretion disks and the production of radio jets. *Mon. Not. R. Astron. Soc.* **1982**, *199*, 883–903. [CrossRef]
6. Bisnovatyi-Kogan, G.S.; Lovelace, R.V.E. Advective accretion disks and related problems including magnetic fields. *New Astron. Rev.* **2001**, *45*, 663–742. [CrossRef]
7. Aloy, M.A.; Rezzolla, L. A Powerful Hydrodynamic Booster for Relativistic Jets. *Astrophys. J. Lett.* **2006**, *640*, L115–L118. [CrossRef]
8. Mizuno, Y.; Hardee, P.; Hartmann, D.H.; Nishikawa, K.I.; Zhang, B. A Magnetohydrodynamic Boost for Relativistic Jets. *Astrophys. J.* **2008**, *672*, 72–82. [CrossRef]
9. Hawley, J.F.; Smarr, L.L.; Wilson, J.R. A numerical study of nonspherical black hole accretion. I Equations and test problems. *Astrophys. J.* **1984**, *277*, 296–311. [CrossRef]
10. Koide, S.; Meier, D.L.; Shibata, K.; Kudoh, T. General Relativistic Simulations of Early Jet Formation in a Rapidly Rotating Black Hole Magnetosphere. *Astrophys. J.* **2000**, *536*, 668–674. [CrossRef]
11. De Villiers, J.P.; Hawley, J.F. A Numerical Method for General Relativistic Magnetohydrodynamics. *Astrophys. J.* **2003**, *589*, 458–480. [CrossRef]
12. Gammie, C.F.; McKinney, J.C.; Tóth, G. HARM: A Numerical Scheme for General Relativistic Magnetohydrodynamics. *Astrophys. J.* **2003**, *589*, 444–457. [CrossRef]
13. Baiotti, L.; Hawke, I.; Montero, P.J.; Löffler, F.; Rezzolla, L.; Stergioulas, N.; Font, J.A.; Seidel, E. Three-dimensional relativistic simulations of rotating neutron-star collapse to a Kerr black hole. *Phys. Rev. D* **2005**, *71*, 024035. [CrossRef]
14. Duez, M.D.; Liu, Y.T.; Shapiro, S.L.; Stephens, B.C. Relativistic magnetohydrodynamics in dynamical spacetimes: Numerical methods and tests. *Phys. Rev. D* **2005**, *72*, 024028. [CrossRef]
15. Anninos, P.; Fragile, P.C.; Salmonson, J.D. Cosmos++: Relativistic Magnetohydrodynamics on Unstructured Grids with Local Adaptive Refinement. *Astrophys. J.* **2005**, *635*, 723–740. [CrossRef]
16. Antón, L.; Zanotti, O.; Miralles, J.A.; Martí, J.M.; Ibáñez, J.M.; Font, J.A.; Pons, J.A. Numerical 3+1 General Relativistic Magnetohydrodynamics: A Local Characteristic Approach. *Astrophys. J.* **2006**, *637*, 296–312. [CrossRef]

17. Mizuno, Y.; Nishikawa, K.I.; Koide, S.; Hardee, P.; Fishman, G.J. RAISHIN: A High-Resolution Three-Dimensional General Relativistic Magnetohydrodynamics Code. *arXiv* **2006**, arXiv:astro-ph/0609004.
18. Del Zanna, L.; Zanotti, O.; Bucciantini, N.; Londrillo, P. ECHO: A Eulerian conservative high-order scheme for general relativistic magnetohydrodynamics and magnetodynamics. *Astron. Astrophys.* **2007**, *473*, 11–30. [CrossRef]
19. Giacomazzo, B.; Rezzolla, L. WhiskyMHD: A new numerical code for general relativistic magnetohydrodynamics. *Class. Quantum Gravity* **2007**, *24*, S235–S258. [CrossRef]
20. Etienne, Z.B.; Paschalidis, V.; Haas, R.; Mösta, P.; Shapiro, S.L. IllinoisGRMHD: An open-source, user-friendly GRMHD code for dynamical spacetimes. *Class. Quantum Gravity* **2015**, *32*, 175009. [CrossRef]
21. White, C.J.; Stone, J.M.; Gammie, C.F. An Extension of the Athena++ Code Framework for GRMHD Based on Advanced Riemann Solvers and Staggered-mesh Constrained Transport. *Astrophys. J. Suppl.* **2016**, *225*, 22. [CrossRef]
22. Zanotti, O.; Dumbser, M. A high order special relativistic hydrodynamic and magnetohydrodynamic code with space-time adaptive mesh refinement. *Comput. Phys. Commun.* **2015**, *188*, 110–127. [CrossRef]
23. Porth, O.; Olivares, H.; Mizuno, Y.; Younsi, Z.; Rezzolla, L.; Moscibrodzka, M.; Falcke, H.; Kramer, M. The black hole accretion code. *Comput. Astrophys. Cosmol.* **2017**, *4*, 1. [CrossRef]
24. Olivares, H.; Porth, O.; Davelaar, J.; Most, E.R.; Fromm, C.M.; Mizuno, Y.; Younsi, Z.; Rezzolla, L. Constrained transport and adaptive mesh refinement in the Black Hole Accretion Code. *Astron. Astrophys.* **2019**, *629*, A61. [CrossRef]
25. Liska, M.; Chatterjee, K.; Tchekhovskoy, A.; Yoon, D.; van Eijnatten, D.; Hesp, C.; Markoff, S.; Ingram, A.; van der Klis, M. H-AMR: A New GPU-accelerated GRMHD Code for Exascale Computing with 3D Adaptive Mesh Refinement and Local Adaptive Time-stepping. *arXiv* **2019**, arXiv:1912.10192.
26. Chi-Kit Cheong, P.; Tsz-Lok Lam, A.; Ho-Yin Ng, H.; Li, T.G.F. Gmunu: Paralleled, grid-adaptive, general-relativistic magnetohydrodynamics in curvilinear geometries in dynamical spacetimes. *arXiv* **2020**, arXiv:2012.07322.
27. Rezzolla, L.; Zanotti, O. *Relativistic Hydrodynamics*; Oxford University Press: Oxford, UK, 2013.
28. Font, J.A. Numerical Hydrodynamics in General Relativity. *Living Rev. Relativ.* **2003**, *6*, 4. [CrossRef]
29. Martí, J.M.; Müller, E. Grid-based Methods in Relativistic Hydrodynamics and Magnetohydrodynamics. *Living Rev. Comput. Astrophys.* **2015**, *1*, 3. [CrossRef]
30. Sądowski, A.; Narayan, R.; Tchekhovskoy, A.; Zhu, Y. Semi-implicit scheme for treating radiation under M1 closure in general relativistic conservative fluid dynamics codes. *Mon. Not. R. Astron. Soc.* **2013**, *429*, 3533–3550. [CrossRef]
31. McKinney, J.C.; Tchekhovskoy, A.; Sadowski, A.; Narayan, R. Three-dimensional general relativistic radiation magnetohydrodynamical simulation of super-Eddington accretion, using a new code HARMRAD with M1 closure. *Mon. Not. R. Astron. Soc.* **2014**, *441*, 3177–3208. [CrossRef]
32. Takahashi, H.R.; Ohsuga, K.; Kawashima, T.; Sekiguchi, Y. Formation of Overheated Regions and Truncated Disks around Black Holes: Three-dimensional General Relativistic Radiation-magnetohydrodynamics Simulations. *Astrophys. J.* **2016**, *826*, 23. [CrossRef]
33. Bucciantini, N.; Del Zanna, L. A fully covariant mean-field dynamo closure for numerical 3 + 1 resistive GRMHD. *Mon. Not. R. Astron. Soc.* **2013**, *428*, 71–85. [CrossRef]
34. Dionysopoulou, K.; Alic, D.; Palenzuela, C.; Rezzolla, L.; Giacomazzo, B. General-relativistic resistive magnetohydrodynamics in three dimensions: Formulation and tests. *Phys. Rev. D* **2013**, *88*, 044020. [CrossRef]
35. Chandra, M.; Gammie, C.F.; Foucart, F.; Quataert, E. An Extended Magnetohydrodynamics Model for Relativistic Weakly Collisional Plasmas. *Astrophys. J.* **2015**, *810*, 162. [CrossRef]
36. Chandra, M.; Foucart, F.; Gammie, C.F. grim: A Flexible, Conservative Scheme for Relativistic Fluid Theories. *Astrophys. J.* **2017**, *837*, 92. [CrossRef]
37. Del Zanna, L.; Bucciantini, N. Covariant and 3 + 1 equations for dynamo-chiral general relativistic magnetohydrodynamics. *Mon. Not. R. Astron. Soc.* **2018**, *479*, 657–666. [CrossRef]
38. Ripperda, B.; Bacchini, F.; Porth, O.; Most, E.R.; Olivares, H.; Nathanail, A.; Rezzolla, L.; Teunissen, J.; Keppens, R. General-relativistic Resistive Magnetohydrodynamics with Robust Primitive-variable Recovery for Accretion Disk Simulations. *Astrophys. J. Suppl.* **2019**, *244*, 10. [CrossRef]
39. Fender, R.P.; Belloni, T.M.; Gallo, E. Towards a unified model for black hole X-ray binary jets. *Mon. Not. R. Astron. Soc.* **2004**, *355*, 1105–1118. [CrossRef]
40. Markoff, S. Sagittarius A* in Context: Daily Flares as a Probe of the Fundamental X-Ray Emission Process in Accreting Black Holes. *Astrophys. J. Lett.* **2005**, *618*, L103–L106. [CrossRef]
41. Marrone, D.P.; Moran, J.M.; Zhao, J.H.; Rao, R. An Unambiguous Detection of Faraday Rotation in Sagittarius A*. *Astrophys. J. Lett.* **2007**, *654*, L57–L60. [CrossRef]
42. Ho, L.C. Radiatively Inefficient Accretion in Nearby Galaxies. *Astrophys. J.* **2009**, *699*, 626–637. [CrossRef]
43. Narayan, R.; Yi, I. Advection-dominated Accretion: A Self-similar Solution. *Astrophys. J. Lett.* **1994**, *428*, L13. [CrossRef]
44. Narayan, R.; Yi, I. Advection-dominated Accretion: Underfed Black Holes and Neutron Stars. *Astrophys. J.* **1995**, *452*, 710. [CrossRef]
45. Abramowicz, M.A.; Chen, X.; Kato, S.; Lasota, J.P.; Regev, O. Thermal Equilibria of Accretion Disks. *Astrophys. J. Lett.* **1995**, *438*, L37. [CrossRef]
46. Yuan, F.; Narayan, R. Hot Accretion Flows Around Black Holes. *Annu. Rev. Astron. Astrophys.* **2014**, *52*, 529–588. [CrossRef]

47. Yuan, F.; Quataert, E.; Narayan, R. Nonthermal Electrons in Radiatively Inefficient Accretion Flow Models of Sagittarius A*. *Astrophys. J.* **2003**, *598*, 301–312. [CrossRef]
48. Novikov, I.D.; Thorne, K.S. Astrophysics of black holes. In *Black Holes (Les Astres Occlus)*; Dewitt, C., Dewitt, B.S., Eds.; Gordon & Breach: New York, NY, USA, 1973; pp. 343–450.
49. Shakura, N.I.; Sunyaev, R.A. Reprint of 1973A&A....24..337S. Black holes in binary systems. Observational appearance. *Astron. Astrophys.* **1973**, *500*, 33–51.
50. Abramowicz, M.A.; Czerny, B.; Lasota, J.P.; Szuszkiewicz, E. Slim Accretion Disks. *Astrophys. J.* **1988**, *332*, 646. [CrossRef]
51. Koide, S.; Shibata, K.; Kudoh, T. General Relativistic Magnetohydrodynamic Simulations of Jets from Black Hole Accretions Disks: Two-Component Jets Driven by Nonsteady Accretion of Magnetized Disks. *Astrophys. J. Lett.* **1998**, *495*, L63–L66. [CrossRef]
52. Koide, S.; Shibata, K.; Kudoh, T. Relativistic Jet Formation from Black Hole Magnetized Accretion Disks: Method, Tests, and Applications of a General RelativisticMagnetohydrodynamic Numerical Code. *Astrophys. J.* **1999**, *522*, 727–752. [CrossRef]
53. Nishikawa, K.I.; Richardson, G.; Koide, S.; Shibata, K.; Kudoh, T.; Hardee, P.; Fishman, G.J. A General Relativistic Magnetohydrodynamic Simulation of Jet Formation. *Astrophys. J.* **2005**, *625*, 60–71. [CrossRef]
54. Hardee, P.; Mizuno, Y.; Nishikawa, K.I. GRMHD/RMHD simulations & stability of magnetized spine-sheath relativistic jets. *Astrophys. Space Sci.* **2007**, *311*, 281–286. [CrossRef]
55. Shafee, R.; McKinney, J.C.; Narayan, R.; Tchekhovskoy, A.; Gammie, C.F.; McClintock, J.E. Three-Dimensional Simulations of Magnetized Thin Accretion Disks around Black Holes: Stress in the Plunging Region. *Astrophys. J. Lett.* **2008**, *687*, L25. [CrossRef]
56. Noble, S.C.; Krolik, J.H.; Hawley, J.F. Dependence of Inner Accretion Disk Stress on Parameters: The Schwarzschild Case. *Astrophys. J.* **2010**, *711*, 959–973. [CrossRef]
57. Noble, S.C.; Krolik, J.H.; Schnittman, J.D.; Hawley, J.F. Radiative Efficiency and Thermal Spectrum of Accretion onto Schwarzschild Black Holes. *Astrophys. J.* **2011**, *743*, 115. [CrossRef]
58. Penna, R.F.; McKinney, J.C.; Narayan, R.; Tchekhovskoy, A.; Shafee, R.; McClintock, J.E. Simulations of magnetized discs around black holes: Effects of black hole spin, disc thickness and magnetic field geometry. *Mon. Not. R. Astron. Soc.* **2010**, *408*, 752–782. [CrossRef]
59. Avara, M.J.; McKinney, J.C.; Reynolds, C.S. Efficiency of thin magnetically arrested discs around black holes. *Mon. Not. R. Astron. Soc.* **2016**, *462*, 636–648. [CrossRef]
60. Dihingia, I.K.; Vaidya, B.; Fendt, C. Jets, disc-winds, and oscillations in general relativistic, magnetically driven flows around black hole. *Mon. Not. R. Astron. Soc.* **2021**, *505*, 3596–3615. [CrossRef]
61. Bardeen, J.M.; Petterson, J.A. The Lense-Thirring Effect and Accretion Disks around Kerr Black Holes. *Astrophys. J. Lett.* **1975**, *195*, L65. [CrossRef]
62. Liska, M.; Hesp, C.; Tchekhovskoy, A.; Ingram, A.; van der Klis, M.; Markoff, S. Formation of precessing jets by tilted black hole discs in 3D general relativistic MHD simulations. *Mon. Not. R. Astron. Soc.* **2018**, *474*, L81–L85. [CrossRef]
63. Liska, M.; Hesp, C.; Tchekhovskoy, A.; Ingram, A.; van der Klis, M.; Markoff, S.B.; Van Moer, M. Disc tearing and Bardeen-Petterson alignment in GRMHD simulations of highly tilted thin accretion discs. *Mon. Not. R. Astron. Soc.* **2021**, *507*, 983–990. [CrossRef]
64. Qian, Q.; Fendt, C.; Vourellis, C. Jet Launching in Resistive GR-MHD Black Hole-Accretion Disk Systems. *Astrophys. J.* **2018**, *859*, 28. [CrossRef]
65. Vourellis, C.; Fendt, C.; Qian, Q.; Noble, S.C. GR-MHD Disk Winds and Jets from Black Holes and Resistive Accretion Disks. *Astrophys. J.* **2019**, *882*, 2. [CrossRef]
66. Balbus, S.A.; Hawley, J.F. A Powerful Local Shear Instability in Weakly Magnetized Disks. I. Linear Analysis. *Astrophys. J.* **1991**, *376*, 214. [CrossRef]
67. Balbus, S.A.; Hawley, J.F. Instability, turbulence, and enhanced transport in accretion disks. *Rev. Mod. Phys.* **1998**, *70*, 1–53. [CrossRef]
68. De Villiers, J.P.; Hawley, J.F. Global General Relativistic Magnetohydrodynamic Simulations of Accretion Tori. *Astrophys. J.* **2003**, *592*, 1060–1077. [CrossRef]
69. McKinney, J.C.; Gammie, C.F. A Measurement of the Electromagnetic Luminosity of a Kerr Black Hole. *Astrophys. J.* **2004**, *611*, 977–995. [CrossRef]
70. McKinney, J.C. General relativistic magnetohydrodynamic simulations of the jet formation and large-scale propagation from black hole accretion systems. *Mon. Not. R. Astron. Soc.* **2006**, *368*, 1561–1582 [CrossRef]
71. McKinney, J.C.; Blandford, R.D. Stability of relativistic jets from rotating, accreting black holes via fully three-dimensional magnetohydrodynamic simulations. *Mon. Not. R. Astron. Soc.* **2009**, *394*, L126–L130. [CrossRef]
72. De Villiers, J.P.; Hawley, J.F.; Krolik, J.H. Magnetically Driven Accretion Flows in the Kerr Metric. I. Models and Overall Structure. *Astrophys. J.* **2003**, *599*, 1238–1253. [CrossRef]
73. De Villiers, J.P.; Hawley, J.F.; Krolik, J.H.; Hirose, S. Magnetically Driven Accretion in the Kerr Metric. III. Unbound Outflows. *Astrophys. J.* **2005**, *620*, 878–888. [CrossRef]
74. Hirose, S.; Krolik, J.H.; De Villiers, J.P.; Hawley, J.F. Magnetically Driven Accretion Flows in the Kerr Metric. II. Structure of the Magnetic Field. *Astrophys. J.* **2004**, *606*, 1083–1097. [CrossRef]
75. Hawley, J.F.; Krolik, J.H. Magnetically Driven Jets in the Kerr Metric. *Astrophys. J.* **2006**, *641*, 103–116. [CrossRef]

76. Beckwith, K.; Hawley, J.F.; Krolik, J.H. The Influence of Magnetic Field Geometry on the Evolution of Black Hole Accretion Flows: Similar Disks, Drastically Different Jets. *Astrophys. J.* **2008**, *678*, 1180–1199. [CrossRef]
77. Narayan, R.; SÄ dowski, A.; Penna, R.F.; Kulkarni, A.K. GRMHD simulations of magnetized advection-dominated accretion on a non-spinning black hole: Role of outflows. *Mon. Not. R. Astron. Soc.* **2012**, *426*, 3241–3259. [CrossRef]
78. Sądowski, A.; Narayan, R.; Penna, R.; Zhu, Y. Energy, momentum and mass outflows and feedback from thick accretion discs around rotating black holes. *Mon. Not. R. Astron. Soc.* **2013**, *436*, 3856–3874. [CrossRef]
79. Porth, O.; Chatterjee, K.; Narayan, R.; Gammie, C.F.; Mizuno, Y.; Anninos, P.; Baker, J.G.; Bugli, M.; Chan, C.k.; Davelaar, J.; et al. The Event Horizon General Relativistic Magnetohydrodynamic Code Comparison Project. *Astrophys. J. Suppl.* **2019**, *243*, 26. [CrossRef]
80. Vlahakis, N.; Königl, A. Relativistic Magnetohydrodynamics with Application to Gamma-Ray Burst Outflows. I. Theory and Semianalytic Trans-Alfvénic Solutions. *Astrophys. J.* **2003**, *596*, 1080–1103. [CrossRef]
81. Beskin, V.S.; Nokhrina, E.E. The effective acceleration of plasma outflow in the paraboloidal magnetic field. *Mon. Not. R. Astron. Soc.* **2006**, *367*, 375–386. [CrossRef]
82. Lyubarsky, Y. Asymptotic Structure of Poynting-Dominated Jets. *Astrophys. J.* **2009**, *698*, 1570–1589. [CrossRef]
83. Pu, H.Y.; Nakamura, M.; Hirotani, K.; Mizuno, Y.; Wu, K.; Asada, K. Steady General Relativistic Magnetohydrodynamic Inflow/Outflow Solution Along Large-Scale Magnetic Fields that Thread a Rotating Black Hole. *Astrophys. J.* **2015**, *801*, 56. [CrossRef]
84. McKinney, J.C.; Narayan, R. Disc-jet coupling in black hole accretion systems—I. General relativistic magnetohydrodynamical models. *Mon. Not. R. Astron. Soc.* **2007**, *375*, 513–530. [CrossRef]
85. Nakamura, M.; Asada, K.; Hada, K.; Pu, H.Y.; Noble, S.; Tseng, C.; Toma, K.; Kino, M.; Nagai, H.; Takahashi, K.; et al. Parabolic Jets from the Spinning Black Hole in M87. *Astrophys. J.* **2018**, *868*, 146. [CrossRef]
86. McKinney, J.C.; Narayan, R. Disc-jet coupling in black hole accretion systems—II. Force-free electrodynamical models. *Mon. Not. R. Astron. Soc.* **2007**, *375*, 531–547. [CrossRef]
87. Komissarov, S.S.; Barkov, M.V.; Vlahakis, N.; Königl, A. Magnetic acceleration of relativistic active galactic nucleus jets. *Mon. Not. R. Astron. Soc.* **2007**, *380*, 51–70. [CrossRef]
88. Komissarov, S.S.; Vlahakis, N.; Königl, A.; Barkov, M.V. Magnetic acceleration of ultrarelativistic jets in gamma-ray burst sources. *Mon. Not. R. Astron. Soc.* **2009**, *394*, 1182–1212. [CrossRef]
89. Tchekhovskoy, A.; McKinney, J.C.; Narayan, R. Simulations of ultrarelativistic magnetodynamic jets from gamma-ray burst engines. *Mon. Not. R. Astron. Soc.* **2008**, *388*, 551–572. [CrossRef]
90. Tchekhovskoy, A.; Narayan, R.; McKinney, J.C. Black Hole Spin and The Radio Loud/Quiet Dichotomy of Active Galactic Nuclei. *Astrophys. J.* **2010**, *711*, 50–63. [CrossRef]
91. Chatterjee, K.; Liska, M.; Tchekhovskoy, A.; Markoff, S.B. Accelerating AGN jets to parsec scales using general relativistic MHD simulations. *Mon. Not. R. Astron. Soc.* **2019**, *490*, 2200–2218. [CrossRef]
92. Begelman, M.C. Instability of Toroidal Magnetic Field in Jets and Plerions. *Astrophys. J.* **1998**, *493*, 291–300. [CrossRef]
93. Giannios, D.; Spruit, H.C. The role of kink instability in Poynting-flux dominated jets. *Astron. Astrophys.* **2006**, *450*, 887–898. [CrossRef]
94. Mizuno, Y.; Lyubarsky, Y.; Nishikawa, K.I.; Hardee, P.E. Three-Dimensional Relativistic Magnetohydrodynamic Simulations of Current-Driven Instability. I. Instability of a Static Column. *Astrophys. J.* **2009**, *700*, 684–693. [CrossRef]
95. Mizuno, Y.; Hardee, P.E.; Nishikawa, K.I. Three-dimensional Relativistic Magnetohydrodynamic Simulations of Current-driven Instability with a Sub-Alfvénic Jet: Temporal Properties. *Astrophys. J.* **2011**, *734*, 19. [CrossRef]
96. Mizuno, Y.; Lyubarsky, Y.; Nishikawa, K.I.; Hardee, P.E. Three-dimensional Relativistic Magnetohydrodynamic Simulations of Current-driven Instability. III. Rotating Relativistic Jets. *Astrophys. J.* **2012**, *757*, 16. [CrossRef]
97. Mizuno, Y.; Hardee, P.E.; Nishikawa, K.I. Spatial Growth of the Current-driven Instability in Relativistic Jets. *Astrophys. J.* **2014**, *784*, 167. [CrossRef]
98. Singh, C.B.; Mizuno, Y.; de Gouveia Dal Pino, E.M. Spatial Growth of Current-driven Instability in Relativistic Rotating Jets and the Search for Magnetic Reconnection. *Astrophys. J.* **2016**, *824*, 48. [CrossRef]
99. Kadowaki, L.H.S.; de Gouveia Dal Pino, E.M.; Medina-Torrejón, T.E.; Mizuno, Y.; Kushwaha, P. Fast Magnetic Reconnection Structures in Poynting Flux-dominated Jets. *Astrophys. J.* **2021**, *912*, 109. [CrossRef]
100. Medina-Torrejón, T.E.; de Gouveia Dal Pino, E.M.; Kadowaki, L.H.S.; Kowal, G.; Singh, C.B.; Mizuno, Y. Particle Acceleration by Relativistic Magnetic Reconnection Driven by Kink Instability Turbulence in Poynting Flux-Dominated Jets. *Astrophys. J.* **2021**, *908*, 193. [CrossRef]
101. Tchekhovskoy, A.; McKinney, J.C.; Narayan, R. Efficiency of Magnetic to Kinetic Energy Conversion in a Monopole Magnetosphere. *Astrophys. J.* **2009**, *699*, 1789–1808. [CrossRef]
102. Komissarov, S.S.; Vlahakis, N.; Königl, A. Rarefaction acceleration of ultrarelativistic magnetized jets in gamma-ray burst sources. *Mon. Not. R. Astron. Soc.* **2010**, *407*, 17–28. [CrossRef]
103. Mizuno, Y.; Gómez, J.L.; Nishikawa, K.I.; Meli, A.; Hardee, P.E.; Rezzolla, L. Recollimation Shocks in Magnetized Relativistic Jets. *Astrophys. J.* **2015**, *809*, 38. [CrossRef]
104. Gómez, J.L.; Lobanov, A.P.; Bruni, G.; Kovalev, Y.Y.; Marscher, A.P.; Jorstad, S.G.; Mizuno, Y.; Bach, U.; Sokolovsky, K.V.; Anderson, J.M.; et al. Probing the Innermost Regions of AGN Jets and Their Magnetic Fields with RadioAstron. I. Imaging BL Lacertae at 21 Microarcsecond Resolution. *Astrophys. J.* **2016**, *817*, 96. [CrossRef]

105. Mizuno, Y.; Younsi, Z.; Fromm, C.M.; Porth, O.; De Laurentis, M.; Olivares, H.; Falcke, H.; Kramer, M.; Rezzolla, L. The current ability to test theories of gravity with black hole shadows. *Nat. Astron.* **2018**, *2*, 585–590. [CrossRef]
106. Olivares, H.; Younsi, Z.; Fromm, C.M.; De Laurentis, M.; Porth, O.; Mizuno, Y.; Falcke, H.; Kramer, M.; Rezzolla, L. How to tell an accreting boson star from a black hole. *Mon. Not. R. Astron. Soc.* **2020**, *497*, 521–535. [CrossRef]
107. Igumenshchev, I.V.; Narayan, R.; Abramowicz, M.A. Three-dimensional Magnetohydrodynamic Simulations of Radiatively Inefficient Accretion Flows. *Astrophys. J.* **2003**, *592*, 1042–1059. [CrossRef]
108. Igumenshchev, I.V. Magnetically Arrested Disks and the Origin of Poynting Jets: A Numerical Study. *Astrophys. J.* **2008**, *677*, 317–326. [CrossRef]
109. Narayan, R.; Igumenshchev, I.V.; Abramowicz, M.A. Magnetically Arrested Disk: An Energetically Efficient Accretion Flow. *Publ. Astron. Soc. Jpn.* **2003**, *55*, L69–L72. [CrossRef]
110. Tchekhovskoy, A.; McKinney, J.C. Prograde and retrograde black holes: Whose jet is more powerful? *Mon. Not. R. Astron. Soc.* **2012**, *423*, L55–L59. [CrossRef]
111. McKinney, J.C.; Tchekhovskoy, A.; Blandford, R.D. General relativistic magnetohydrodynamic simulations of magnetically choked accretion flows around black holes. *Mon. Not. R. Astron. Soc.* **2012**, *423*, 3083–3117. [CrossRef]
112. Tchekhovskoy, A.; Narayan, R.; McKinney, J.C. Efficient generation of jets from magnetically arrested accretion on a rapidly spinning black hole. *Mon. Not. R. Astron. Soc.* **2011**, *418*, L79–L83. [CrossRef]
113. White, C.J.; Stone, J.M.; Quataert, E. A Resolution Study of Magnetically Arrested Disks. *Astrophys. J.* **2019**, *874*, 168. [CrossRef]
114. Narayan, R.; Chael, A.; Chatterjee, K.; Ricarte, A.; Curd, B. Jets in Magnetically Arrested Hot Accretion Flows: Geometry, Power and Black Hole Spindown. *arXiv* **2021**, arXiv:2108.12380.
115. Fromm, C.M.; Cruz-Osorio, A.; Mizuno, Y.; Nathanail, A.; Younsi, Z.; Porth, O.; Davelaar, J.; Falke, H.; Kramer, M.; Rezzolla, L. Impact of non-thermal particles on the spectral and structural properties of M87. *Astron. Astrophys.* 2021, *submitted*.
116. Dexter, J.; Jiménez-Rosales, A.; Ressler, S.M.; Tchekhovskoy, A.; Bauböck, M.; de Zeeuw, P.T.; Eisenhauer, F.; von Fellenberg, S.; Gao, F.; Genzel, R.; et al. A parameter survey of Sgr A* radiative models from GRMHD simulations with self-consistent electron heating. *Mon. Not. R. Astron. Soc.* **2020**, *494*, 4168–4186. [CrossRef]
117. Porth, O.; Mizuno, Y.; Younsi, Z.; Fromm, C.M. Flares in the Galactic Centre—I. Orbiting flux tubes in magnetically arrested black hole accretion discs. *Mon. Not. R. Astron. Soc.* **2021**, *502*, 2023–2032. [CrossRef]
118. Wong, G.N.; Du, Y.; Prather, B.S.; Gammie, C.F. The Jet-disk Boundary Layer in Black Hole Accretion. *Astrophys. J.* **2021**, *914*, 55 [CrossRef]
119. Event Horizon Telescope Collaboration; Akiyama, K.; Algaba, J.C.; Alberdi, A.; Alef, W.; Anantua, R.; Asada, K.; Azulay, R.; Baczko, A.K.; Ball, D.; et al. First M87 Event Horizon Telescope Results. VIII. Magnetic Field Structure near The Event Horizon. *Astrophys. J. Lett.* **2021**, *910*, L13. [CrossRef]
120. Zamaninasab, M.; Clausen-Brown, E.; Savolainen, T.; Tchekhovskoy, A. Dynamically important magnetic fields near accreting supermassive black holes. *Nature* **2014**, *510*, 126–128. [CrossRef] [PubMed]
121. Nemmen, R.S.; Tchekhovskoy, A. On the efficiency of jet production in radio galaxies. *Mon. Not. R. Astron. Soc.* **2015**, *449*, 316–327. [CrossRef]
122. Beckwith, K.; Hawley, J.F.; Krolik, J.H. Transport of Large-Scale Poloidal Flux in Black Hole Accretion. *Astrophys. J.* **2009**, *707*, 428–445. [CrossRef]
123. Barkov, M.V.; Baushev, A.N. Accretion of a massive magnetized torus on a rotating black hole. *New Astron.* **2011**, *16*, 46–56. [CrossRef]
124. White, C.J.; Quataert, E.; Gammie, C.F. The Structure of Radiatively Inefficient Black Hole Accretion Flows. *Astrophys. J.* **2020**, *891*, 63. [CrossRef]
125. Nathanail, A.; Fromm, C.M.; Porth, O.; Olivares, H.; Younsi, Z.; Mizuno, Y.; Rezzolla, L. Plasmoid formation in global GRMHD simulations and AGN flares. *Mon. Not. R. Astron. Soc.* **2020**, *495*, 1549–1565. [CrossRef]
126. Nathanail, A.; Mpisketzis, V.; Porth, O.; Fromm, C.M.; Rezzolla, L. Magnetic reconnection and plasmoid formation in three-dimensional accretion flows around black holes. *arXiv* **2021**, arXiv:2111.03689.
127. Ripperda, B.; Bacchini, F.; Philippov, A.A. Magnetic Reconnection and Hot Spot Formation in Black Hole Accretion Disks. *Astrophys. J.* **2020**, *900*, 100. [CrossRef]
128. Chashkina, A.; Bromberg, O.; Levinson, A. GRMHD simulations of BH activation by small scale magnetic loops: Formation of striped jets and active coronae. *Mon. Not. R. Astron. Soc.* **2021**, *508*, 1241–1252. [CrossRef]
129. Brandenburg, A.; Nordlund, A.; Stein, R.F.; Torkelsson, U. Dynamo-generated Turbulence and Large-Scale Magnetic Fields in a Keplerian Shear Flow. *Astrophys. J.* **1995**, *446*, 741. [CrossRef]
130. Liska, M.; Tchekhovskoy, A.; Quataert, E. Large-scale poloidal magnetic field dynamo leads to powerful jets in GRMHD simulations of black hole accretion with toroidal field. *Mon. Not. R. Astron. Soc.* **2020**, *494*, 3656–3662. [CrossRef]
131. Komissarov, S.S. Magnetized tori around Kerr black holes: Analytic solutions with a toroidal magnetic field. *Mon. Not. R. Astron. Soc.* **2006**, *368*, 993–1000. [CrossRef]
132. Wielgus, M.; Fragile, P.C.; Wang, Z.; Wilson, J. Local stability of strongly magnetized black hole tori. *Mon. Not. R. Astron. Soc.* **2015**, *447*, 3593–3601. [CrossRef]
133. Fragile, P.C.; Sądowski, A. On the decay of strong magnetization in global disc simulations with toroidal fields. *Mon. Not. R. Astron. Soc.* **2017**, *467*, 1838–1843. [CrossRef]

134. Bugli, M.; Guilet, J.; Müller, E.; Del Zanna, L.; Bucciantini, N.; Montero, P.J. Papaloizou-Pringle instability suppression by the magnetorotational instability in relativistic accretion discs. *Mon. Not. R. Astron. Soc.* **2018**, *475*, 108–120. [CrossRef]
135. Fragile, P.C.; Blaes, O.M.; Anninos, P.; Salmonson, J.D. Global General Relativistic Magnetohydrodynamic Simulation of a Tilted Black Hole Accretion Disk. *Astrophys. J.* **2007**, *668*, 417–429. [CrossRef]
136. Fragile, P.C.; Blaes, O.M. Epicyclic Motions and Standing Shocks in Numerically Simulated Tilted Black Hole Accretion Disks. *Astrophys. J.* **2008**, *687*, 757–766. [CrossRef]
137. White, C.J.; Quataert, E.; Blaes, O. Tilted Disks around Black Holes: A Numerical Parameter Survey for Spin and Inclination Angle. *Astrophys. J.* **2019**, *878*, 51. [CrossRef]
138. Chatterjee, K.; Younsi, Z.; Liska, M.; Tchekhovskoy, A.; Markoff, S.B.; Yoon, D.; van Eijnatten, D.; Hesp, C.; Ingram, A.; van der Klis, M.B.M. Observational signatures of disc and jet misalignment in images of accreting black holes. *Mon. Not. R. Astron. Soc.* **2020**, *499*, 362–378. [CrossRef]
139. Mahadevan, R.; Quataert, E. Are Particles in Advection-dominated Accretion Flows Thermal? *Astrophys. J.* **1997**, *490*, 605–618. [CrossRef]
140. Foucart, F.; Chandra, M.; Gammie, C.F.; Quataert, E. Evolution of accretion discs around a kerr black hole using extended magnetohydrodynamics. *Mon. Not. R. Astron. Soc.* **2016**, *456*, 1332–1345. [CrossRef]
141. Foucart, F.; Chandra, M.; Gammie, C.F.; Quataert, E.; Tchekhovskoy, A. How important is non-ideal physics in simulations of sub-Eddington accretion on to spinning black holes? *Mon. Not. R. Astron. Soc.* **2017**, *470*, 2240–2252. [CrossRef]
142. Tomei, N.; Del Zanna, L.; Bugli, M.; Bucciantini, N. General relativistic magnetohydrodynamic dynamo in thick accretion discs: Fully non-linear simulations. *Mon. Not. R. Astron. Soc.* **2020**, *491*, 2346–2359. [CrossRef]
143. Bugli, M.; Del Zanna, L.; Bucciantini, N. Dynamo action in thick discs around Kerr black holes: High-order resistive GRMHD simulations. *Mon. Not. R. Astron. Soc.* **2014**, *440*, L41–L45. [CrossRef]
144. Fragile, P.C.; Meier, D.L. General Relativistic Magnetohydrodynamic Simulations of the Hard State as a Magnetically Dominated Accretion Flow. *Astrophys. J.* **2009**, *693*, 771–783. [CrossRef]
145. Dibi, S.; Drappeau, S.; Fragile, P.C.; Markoff, S.; Dexter, J. General relativistic magnetohydrodynamic simulations of accretion on to Sgr A*: How important are radiative losses? *Mon. Not. R. Astron. Soc.* **2012**, *426*, 1928–1939. [CrossRef]
146. Yoon, D.; Chatterjee, K.; Markoff, S.B.; van Eijnatten, D.; Younsi, Z.; Liska, M.; Tchekhovskoy, A. Spectral and imaging properties of Sgr A* from high-resolution 3D GRMHD simulations with radiative cooling. *Mon. Not. R. Astron. Soc.* **2020**, *499*, 3178–3192. [CrossRef]
147. Ryan, B.R.; Dolence, J.C.; Gammie, C.F. bhlight: General Relativistic Radiation Magnetohydrodynamics with Monte Carlo Transport. *Astrophys. J.* **2015**, *807*, 31. [CrossRef]
148. Ryan, B.R.; Ressler, S.M.; Dolence, J.C.; Tchekhovskoy, A.; Gammie, C.; Quataert, E. The Radiative Efficiency and Spectra of Slowly Accreting Black Holes from Two-temperature GRRMHD Simulations. *Astrophys. J. Lett.* **2017**, *844*, L24. [CrossRef]
149. Ryan, B.R.; Ressler, S.M.; Dolence, J.C.; Gammie, C.; Quataert, E. Two-temperature GRRMHD Simulations of M87. *Astrophys. J.* **2018**, *864*, 126. [CrossRef]
150. Yao, P.Z.; Dexter, J.; Chen, A.Y.; Ryan, B.R.; Wong, G.N. Radiation GRMHD simulations of M87: Funnel properties and prospects for gap acceleration. *Mon. Not. R. Astron. Soc.* **2021**, *507*, 4864–4878. [CrossRef]
151. Farris, B.D.; Li, T.K.; Liu, Y.T.; Shapiro, S.L. Relativistic radiation magnetohydrodynamics in dynamical spacetimes: Numerical methods and tests. *Phys. Rev. D* **2008**, *78*, 024023. [CrossRef]
152. Fragile, P.C.; Gillespie, A.; Monahan, T.; Rodriguez, M.; Anninos, P. Numerical Simulations of Optically Thick Accretion onto a Black Hole. I. Spherical Case. *Astrophys. J. Suppl.* **2012**, *201*, 9. [CrossRef]
153. Sądowski, A.; Narayan, R.; McKinney, J.C.; Tchekhovskoy, A. Numerical simulations of super-critical black hole accretion flows in general relativity. *Mon. Not. R. Astron. Soc.* **2014**, *439*, 503–520. [CrossRef]
154. Sądowski, A.; Narayan, R.; Tchekhovskoy, A.; Abarca, D.; Zhu, Y.; McKinney, J.C. Global simulations of axisymmetric radiative black hole accretion discs in general relativity with a mean-field magnetic dynamo. *Mon. Not. R. Astron. Soc.* **2015**, *447*, 49–71. [CrossRef]
155. McKinney, J.C.; Dai, L.; Avara, M.J. Efficiency of super-Eddington magnetically-arrested accretion. *Mon. Not. R. Astron. Soc.* **2015**, *454*, L6–L10. [CrossRef]
156. Sądowski, A.; Narayan, R. Three-dimensional simulations of supercritical black hole accretion discs—Luminosities, photon trapping and variability. *Mon. Not. R. Astron. Soc.* **2016**, *456*, 3929–3947. [CrossRef]
157. Mizuno, Y.; Yamada, S.; Koide, S.; Shibata, K. General Relativistic Magnetohydrodynamic Simulations of Collapsars. *Astrophys. J.* **2004**, *606*, 395–412. [CrossRef]
158. Mizuno, Y.; Yamada, S.; Koide, S.; Shibata, K. General Relativistic Magnetohydrodynamic Simulations of Collapsars: Rotating Black Hole Cases. *Astrophys. J.* **2004**, *615*, 389–401. [CrossRef]
159. Garain, S.K.; Balsara, D.S.; Chakrabarti, S.K.; Kim, J. Effects of Magnetic Field Loops on the Dynamics of Advective Accretion Flows and Jets around a Schwarzschild Black Hole. *Astrophys. J.* **2020**, *888*, 59. [CrossRef]
160. Ressler, S.M.; Quataert, E.; White, C.J.; Blaes, O. Magnetically modified spherical accretion in GRMHD: Reconnection-driven convection and jet propagation. *Mon. Not. R. Astron. Soc.* **2021**, *504*, 6076–6095. [CrossRef]
161. Ressler, S.M.; White, C.J.; Quataert, E.; Stone, J.M. Ab Initio Horizon-scale Simulations of Magnetically Arrested Accretion in Sagittarius A* Fed by Stellar Winds. *Astrophys. J. Lett.* **2020**, *896*, L6. [CrossRef]

162. Ressler, S.M.; Quataert, E.; Stone, J.M. The surprisingly small impact of magnetic fields on the inner accretion flow of Sagittarius A* fueled by stellar winds. *Mon. Not. R. Astron. Soc.* **2020**, *492*, 3272–3293. [CrossRef]
163. Goddi, C.; Falcke, H.; Kramer, M.; Rezzolla, L.; Brinkerink, C.; Bronzwaer, T.; Davelaar, J.R.J.; Deane, R.; de Laurentis, M.; Desvignes, G.; et al. BlackHoleCam: Fundamental physics of the galactic center. *Int. J. Mod. Phys. D* **2017**, *26*, 1730001-239. [CrossRef]
164. Younsi, Z.; Zhidenko, A.; Rezzolla, L.; Konoplya, R.; Mizuno, Y. New method for shadow calculations: Application to parametrized axisymmetric black holes. *Phys. Rev. D* **2016**, *94*, 084025. [CrossRef]
165. Bronzwaer, T.; Davelaar, J.; Younsi, Z.; Mościbrodzka, M.; Olivares, H.; Mizuno, Y.; Vos, J.; Falcke, H. Visibility of black hole shadows in low-luminosity AGN. *Mon. Not. R. Astron. Soc.* **2021**, *501*, 4722–4747. [CrossRef]
166. Fuerst, S.V.; Wu, K. Radiation transfer of emission lines in curved space-time. *Astron. Astrophys.* **2004**, *424*, 733–746. [CrossRef]
167. Noble, S.C.; Leung, P.K.; Gammie, C.F.; Book, L.G. Simulating the emission and outflows from accretion discs. *Class. Quantum Gravity* **2007**, *24*, S259–S274. [CrossRef]
168. Dexter, J.; Agol, E. A Fast New Public Code for Computing Photon Orbits in a Kerr Spacetime. *Astrophys. J.* **2009**, *696*, 1616–1629. [CrossRef]
169. Younsi, Z.; Wu, K.; Fuerst, S.V. General relativistic radiative transfer: Formulation and emission from structured tori around black holes. *Astron. Astrophys.* **2012**, *545*, A13. [CrossRef]
170. Chan, C.k.; Psaltis, D.; Özel, F. GRay: A Massively Parallel GPU-based Code for Ray Tracing in Relativistic Spacetimes. *Astrophys. J.* **2013**, *777*, 13. [CrossRef]
171. Dexter, J. A public code for general relativistic, polarised radiative transfer around spinning black holes. *Mon. Not. R. Astron. Soc.* **2016**, *462*, 115–136. [CrossRef]
172. Chan, C.k.; Medeiros, L.; Özel, F.; Psaltis, D. GRay2: A General Purpose Geodesic Integrator for Kerr Spacetimes. *Astrophys. J.* **2018**, *867*, 59. [CrossRef]
173. Pu, H.Y.; Yun, K.; Younsi, Z.; Yoon, S.J. Odyssey: A Public GPU-based Code for General Relativistic Radiative Transfer in Kerr Spacetime. *Astrophys. J.* **2016**, *820*, 105. [CrossRef]
174. Bronzwaer, T.; Davelaar, J.; Younsi, Z.; Mościbrodzka, M.; Falcke, H.; Kramer, M.; Rezzolla, L. RAPTOR. I. Time-dependent radiative transfer in arbitrary spacetimes. *Astron. Astrophys.* **2018**, *613*, A2. [CrossRef]
175. Mościbrodzka, M.; Gammie, C.F. IPOLE—Semi-analytic scheme for relativistic polarized radiative transport. *Mon. Not. R. Astron. Soc.* **2018**, *475*, 43–54. [CrossRef]
176. Bronzwaer, T.; Younsi, Z.; Davelaar, J.; Falcke, H. RAPTOR. II. Polarized radiative transfer in curved spacetime. *Astron. Astrophys.* **2020**, *641*, A126. [CrossRef]
177. Kawashima, T.; Ohsuga, K.; Takahashi, H.R. RAIKOU: A General Relativistic, Multi-wavelength Radiative Transfer Code. *arXiv* **2021**, arXiv:2108.05131.
178. Broderick, A.E.; Loeb, A. Imaging the Black Hole Silhouette of M87: Implications for Jet Formation and Black Hole Spin. *Astrophys. J.* **2009**, *697*, 1164–1179. [CrossRef]
179. Lu, R.S.; Broderick, A.E.; Baron, F.; Monnier, J.D.; Fish, V.L.; Doeleman, S.S.; Pankratius, V. Imaging the Supermassive Black Hole Shadow and Jet Base of M87 with the Event Horizon Telescope. *Astrophys. J.* **2014**, *788*, 120. [CrossRef]
180. Jeter, B.; Broderick, A.E.; Gold, R. Differentiating disc and black hole-driven jets with EHT images of variability in M87. *Mon. Not. R. Astron. Soc.* **2020**, *493*, 5606–5616. [CrossRef]
181. Takahashi, K.; Toma, K.; Kino, M.; Nakamura, M.; Hada, K. Fast-spinning Black Holes Inferred from Symmetrically Limb-brightened Radio Jets. *Astrophys. J.* **2018**, *868*, 82. [CrossRef]
182. Pu, H.Y.; Wu, K.; Younsi, Z.; Asada, K.; Mizuno, Y.; Nakamura, M. Observable Emission Features of Black Hole GRMHD Jets on Event Horizon Scales. *Astrophys. J.* **2017**, *845*, 160. [CrossRef]
183. Shcherbakov, R.V.; Penna, R.F.; McKinney, J.C. Sagittarius A* Accretion Flow and Black Hole Parameters from General Relativistic Dynamical and Polarized Radiative Modeling. *Astrophys. J.* **2012**, *755*, 133. [CrossRef]
184. Dexter, J.; McKinney, J.C.; Agol, E. The size of the jet launching region in M87. *Mon. Not. R. Astron. Soc.* **2012**, *421*, 1517–1528. [CrossRef]
185. Mościbrodzka, M.; Falcke, H.; Shiokawa, H.; Gammie, C.F. Observational appearance of inefficient accretion flows and jets in 3D GRMHD simulations: Application to Sagittarius A*. *Astron. Astrophys.* **2014**, *570*, A7. [CrossRef]
186. Mościbrodzka, M.; Falcke, H.; Shiokawa, H. General relativistic magnetohydrodynamical simulations of the jet in M 87. *Astron. Astrophys.* **2016**, *586*, A38. [CrossRef]
187. Chan, C.K.; Psaltis, D.; Özel, F.; Narayan, R.; Sadowski, A. The Power of Imaging: Constraining the Plasma Properties of GRMHD Simulations using EHT Observations of Sgr A*. *Astrophys. J.* **2015**, *799*, 1. [CrossRef]
188. Gold, R.; McKinney, J.C.; Johnson, M.D.; Doeleman, S.S. Probing the Magnetic Field Structure in Sgr A* on Black Hole Horizon Scales with Polarized Radiative Transfer Simulations. *Astrophys. J.* **2017**, *837*, 18. [CrossRef]
189. Mościbrodzka, M.; Falcke, H. Coupled jet-disk model for Sagittarius A*: Explaining the flat-spectrum radio core with GRMHD simulations of jets. *Astron. Astrophys.* **2013**, *559*, L3. [CrossRef]
190. Sharma, P.; Quataert, E.; Hammett, G.W.; Stone, J.M. Electron Heating in Hot Accretion Flows. *Astrophys. J.* **2007**, *667*, 714–723. [CrossRef]
191. Anantua, R.; Ressler, S.; Quataert, E. On the comparison of AGN with GRMHD simulations: I. Sgr A*. *Mon. Not. R. Astron. Soc.* **2020**, *493*, 1404–1418. [CrossRef]

192. Ressler, S.M.; Tchekhovskoy, A.; Quataert, E.; Chandra, M.; Gammie, C.F. Electron thermodynamics in GRMHD simulations of low-luminosity black hole accretion. *Mon. Not. R. Astron. Soc.* **2015**, *454*, 1848–1870. [CrossRef]
193. Mizuno, Y.; Fromm, C.M.; Younsi, Z.; Porth, O.; Olivares, H.; Rezzolla, L. Comparison of the ion-to-electron temperature ratio prescription: GRMHD simulations with electron thermodynamics. *Mon. Not. R. Astron. Soc.* **2021**, *506*, 741–758. [CrossRef]
194. Chael, A.; Narayan, R.; Johnson, M.D. Two-temperature, Magnetically Arrested Disc simulations of the jet from the supermassive black hole in M87. *Mon. Not. R. Astron. Soc.* **2019**, *486*, 2873–2895. [CrossRef]
195. Chael, A.; Rowan, M.; Narayan, R.; Johnson, M.; Sironi, L. The role of electron heating physics in images and variability of the Galactic Centre black hole Sagittarius A*. *Mon. Not. R. Astron. Soc.* **2018**, *478*, 5209–5229. [CrossRef]
196. Howes, G.G. A prescription for the turbulent heating of astrophysical plasmas. *Mon. Not. R. Astron. Soc.* **2010**, *409*, L104–L108. [CrossRef]
197. Kawazura, Y.; Barnes, M.; Schekochihin, A.A. Thermal disequilibration of ions and electrons by collisionless plasma turbulence. *Proc. Natl. Acad. Sci. USA* **2019**, *116*, 771–776. [CrossRef]
198. Rowan, M.E.; Sironi, L.; Narayan, R. Electron and Proton Heating in Transrelativistic Magnetic Reconnection. *Astrophys. J.* **2017**, *850*, 29. [CrossRef]
199. Rowan, M.E.; Sironi, L.; Narayan, R. Electron and Proton Heating in Transrelativistic Guide Field Reconnection. *Astrophys. J.* **2019**, *873*, 2. [CrossRef]
200. Cruz-Osorio, A.; Fromm, C.M.; Mizuno, Y.; Nathanail, A.; Younsi, Z.; Porth, O.; Davelaar, J.; Falke, H.; Kramer, M.; Rezzolla, L. Accurate energetic and morphological modelling of the launching site of the M87 jet. *Nat. Astron.* 2021, *accepted*.
201. Davelaar, J.; Mościbrodzka, M.; Bronzwaer, T.; Falcke, H. General relativistic magnetohydrodynamical κ-jet models for Sagittarius A*. *Astron. Astrophys.* **2018**, *612*, A34. [CrossRef]
202. Vasyliunas, V.M. A survey of low-energy electrons in the evening sector of the magnetosphere with OGO 1 and OGO 3. *J. Geophys. Res.* **1968**, *73*, 2839–2884. [CrossRef]
203. Xiao, F. Modelling energetic particles by a relativistic kappa-loss-cone distribution function in plasmas. *Plasma Phys. Control. Fusion* **2006**, *48*, 203–213. [CrossRef]
204. Pandya, A.; Zhang, Z.; Chandra, M.; Gammie, C.F. Polarized Synchrotron Emissivities and Absorptivities for Relativistic Thermal, Power-law, and Kappa Distribution Functions. *Astrophys. J.* **2016**, *822*, 34. [CrossRef]
205. Marszewski, A.; Prather, B.S.; Joshi, A.V.; Pandya, A.; Gammie, C.F. Updated Transfer Coefficients for Magnetized Plasmas. *arXiv* **2021**, arXiv:2108.10359.
206. Davelaar, J.; Olivares, H.; Porth, O.; Bronzwaer, T.; Janssen, M.; Roelofs, F.; Mizuno, Y.; Fromm, C.M.; Falcke, H.; Rezzolla, L. Modeling non-thermal emission from the jet-launching region of M 87 with adaptive mesh refinement. *Astron. Astrophys.* **2019**, *632*, A2. [CrossRef]
207. Ball, D.; Sironi, L.; Özel, F. Electron and Proton Acceleration in Trans-relativistic Magnetic Reconnection: Dependence on Plasma Beta and Magnetization. *Astrophys. J.* **2018**, *862*, 80. [CrossRef]
208. Kim, J.Y.; Krichbaum, T.P.; Lu, R.S.; Ros, E.; Bach, U.; Bremer, M.; de Vicente, P.; Lindqvist, M.; Zensus, J.A. The limb-brightened jet of M87 down to the 7 Schwarzschild radii scale. *Astron. Astrophys.* **2018**, *616*, A188. [CrossRef]